Durable responses to ATR inhibition with ceralasertib in tumors with genomic defects and high inflammation

Magnus T Dillon[1,2*], Jeane Guevara[2], Kabir Mohammed[2], Emmanuel Christian Patin[1], Simon A. Smith[3], Emma Dean[3], Gemma N Jones[3], Sophie E Willis[3], Marcella Petrone[4], Carlos Silva[4], Khin Thway[2], Catey Bunce[2], Ioannis Roxanis[1], Pablo Nenclares[1], Anna Wilkins[1,2], Martin McLaughlin[1], Adoracion Jayme Laiche[5], Sarah Benafif[5], Georgios Nintos[6], Vineet Kwatra[6], Lorna Grove[1], David Mansfield[1], Paula Proszek[1,2], Philip Martin[7], Luiza Moore[7], Karen Swales[1], Udai Banerji[1,2], Mark Saunders[8], James Spicer[6], Martin D Forster[5†], Kevin J Harrington[1,2†]

1. The Institute of Cancer Research; London, UK
2. The Royal Marsden NHS Foundation Trust; London, UK
3. Oncology R&D, AstraZeneca; Cambridge, UK
4. Clinical Pharmacology and Quantitative Pharmacology, Clinical Pharmacology and Safety Sciences, R&D; AstraZeneca, Cambridge, UK
5. UCL Cancer Institute and University College London Hospital NHS Foundation Trust; London, UK
6. King's College London, and Guy's and St Thomas' NHS Foundation Trust; London, UK
7. Oncology R&D, AstraZeneca; Gaithersburg, Maryland, US
8. The Christie NHS Foundation Trust; Manchester, UK

† Joint senior authors

* Corresponding author address:

The Institute of Cancer Research, Cotswold Road, Sutton, SM2 5NG, United Kingdom.

Magnus.dillon@icr.ac.uk +442073528133

Abstract

Background: PATRIOT was the first-in-human phase I study of the oral ATR (ataxia telangiectasia and Rad3-related) inhibitor ceralasertib (AZD6738) in advanced solid tumors.

Methods: Primary objective was safety. Secondary objectives included assessment of anti-tumor responses, pharmacokinetic (PK) and pharmacodynamic (PD) studies. Sixty-seven patients received ceralasertib 20-240 mg BD continuously or intermittently (14 of a 28-day cycle).

Results: Intermittent dosing was better tolerated than continuous, which was associated with dose-limiting hematological toxicity. The recommended phase 2 dose of ceralasertib was 160 mg twice daily for 2 weeks in a 4-weekly cycle. Modulation of target and increased DNA damage were identified in tumor and surrogate PD. There were 5 (8%) confirmed partial responses (PR, 40-240 mg BD), 34 (52%) stable disease (SD) including 1 unconfirmed partial response, and 27 (41%) progressive disease. Durable responses were seen in tumors with loss of AT-rich interactive domain-containing protein 1A (ARID1A) and DNA damage response defects. Treatment modulated tumor and systemic immune markers and responding tumors were more immune-inflamed than non-responding.

Conclusion: Ceralasertib monotherapy was tolerated at 160 mg BD intermittent and associated with anti-tumor activity.

Trial registration: Clinicaltrials.gov: NCT02223923, EudraCT: 2013-003994-84

Funding: Cancer Research UK, AstraZeneca, UK Department of Health (National Institute for Health Research), Rosetrees Trust, Experimental Cancer Medicine Centre

Role of funding source: AstraZeneca provided funding for components of the clinical conduct of PATRIOT and drug supply and labelling.

Introduction

ATR (ataxia telangiectasia and Rad3-related is a critical kinase in the DNA damage response (DDR)(1, 2). Pre-clinical data have identified multiple cancer-related phenotypes sensitizing tumor cells to monotherapy ATR inhibition (ATRi) (3). Additionally, ATRi potentiates DNA-damaging therapies, including chemotherapy, radiotherapy (4), and targeted therapies such as PARP (poly ADP-ribose polymerase) inhibitors (5), making it a promising combination partner. Emerging evidence suggests ATRi may also modulate anti-tumor immune responses (6-8).

ATR is activated by diverse DNA lesions causing exposure of expanses of single-stranded DNA (2). This replication stress is a frequent consequence of oncogene activation and impaired G1 checkpoint control, and can be secondary to exogenous and endogenous sources of DNA damage and repair. Activated ATR phosphorylates targets including checkpoint kinase 1 (Chk1), leading to stabilization of replication forks, activation of DNA repair, and activation of cell cycle checkpoints (Fig. 1B). Hence, monotherapy ATRi is predicted to impact tumors with high levels of replication stress, reduced DNA repair, or non-functional cell cycle checkpoints leading to accumulation of DNA damage and cell death.

In pre-clinical models, ATRi kills tumor cells with loss of ataxia telangiectasia mutated (ATM) (9), AT-rich interactive domain-containing protein 1A (ARID1A) (10), and specific components of the DDR pathway (11-13) or those driven by oncogenes such as cyclin E and Myc (14-16). Emerging data suggest that increasing the DNA damage load in cells could promote an anti-tumor immune response, for example through interferogenic nucleic acid-sensing pathways (17).

Ceralasertib (AZD6738, AstraZeneca) (18) is a potent, selective, orally bioavailable, ATP-competitive ATR inhibitor, with anti-tumor activity demonstrated in multiple preclinical models (19). We report the results of the PATRIOT study (20), a first-in-human dose-finding study which determined safety, tolerability, recommended dose and schedule, pharmacokinetics (PK) and antitumor activity of ceralasertib monotherapy and explored potential predictive biomarkers of response to ATRi.

Results

Patient characteristics

A total of 26 patients were enrolled and started ceralasertib in the dose-escalation phase across 3 centers between July 2014 and July 2016. In the dose-expansion phase, 43 patients were enrolled, of whom 41 received at least 1 dose of study drug (2 progressed prior to treatment start) between December 2016 and October 2020 (Fig. 1A). Patient and tumor characteristics are given in table 1.

Dose escalation and Toxicity

A total of 67 patients received a dose of ceralasertib and were evaluable for safety (Fig 1A). Twenty-six patients were treated with continuous dosing schedule during the dose-escalation phase, at doses from 20 to 240 mg BD (Fig. 1C). At the maximum administered dose of 240 mg BD, 3/6 patients had DLT. There were no DLTs at 160 mg BD, and one at 80 mg BD (G3 thrombocytopenia with epistaxis, Table 2, Supp. Table 2). The maximum tolerated dose is 160 mg BD. DLTs were thrombocytopenia (G4, n = 2 at 240 mg, G3 with epistaxis, n = 1 at 80 mg), and elevated amylase (G3, n = 1 at 240 mg, Supp. Table 2). Dose expansion participants received 160 mg BD, either continuously or on a 2-week-on, 2-week-off schedule (Fig. 1C). This was investigated after the development of toxicity beyond the DLT window in continuously-dosed patients, leading to dose modifications. The intermittent schedule was chosen based on modelling of bone marrow recovery and was better tolerated, with incidence of G≥3 anemia 33% on continuous vs. 9% on intermittent schedule; 8% vs. 0 % G3 leukopenia. Platelets and other hematological parameters were also more favorable with an intermittent schedule, recovering in the treatment break (Fig. 2A, Table 2, Supp. Fig 1) (21). Six of twelve (50%) patients on the continuous schedule (including those in part A) vs. 10/35 (29%) on the intermittent required dose reduction or interruption for toxicity. Four patients in the dose-

escalation and 1 in dose-expansion phase withdrew due to toxicity. There were no treatment-related deaths. Four deaths occurred on study medication, 2 disease progression, 1 pneumonia and 1 adult respiratory syndrome assumed to be COVID-19 related (no leukopenia observed for the latter 2 participants). The RP2D for the intermittent schedule is 160 mg BD, although other doses were not evaluated on an intermittent schedule.

Serious adverse events related to study treatment are shown in supplementary table 1.

Pharmacokinetics

Ceralasertib was rapidly orally absorbed across all doses following single and multiple dose administration (median t_{max} 0.5 - 4 h), with mean terminal elimination half-life 5.3 – 7.7 h at the 40 and 80 mg dose levels and 11.2 - 12.8 h at the 160 and 240 mg dose levels. Following single dosing, Ceralasertib exposure increased approximately proportionally with increasing doses between 80 – 240 mg (fig. 2B). There was some evidence for accumulation after repeated dosing with higher pre-dose and C_{max} levels at day 15 and 29, compared with day 0. Accumulation ratios based on C_{max} and AUC were between 1.6 and 2.2-fold higher (Supp Fig 2).

Pharmacodynamics

Paired PBMC were available for the majority of study participants. PBMC were analyzed for pChk1, the downstream phosphorylation target of ATR. There was variation in pChk1 levels with treatment, but this was not consistent (Supp. Fig. 3). pChk1 has been described to decrease with ATRi in the presence of exogenous DNA damage (4), and to increase with ATRi reflective of replication stress and DNA damage (22). Increased γH2AX positivity was observed in PBMC after treatment at the RP2D for most subjects (Fig. 2C), likely reflecting DNA damage

in proliferating bone marrow cells due to ATRi. Four paired tumor biopsies were available for IHC. These tumor biopsies showed upregulation of pRad50, a marker of ATM pathway activation, after treatment with ceralasertib (Fig. 2D, 2E), as well as an increase in the number of γH2AX-positive cells (Fig. 2F, 2G).

Response

At data cut-off, 4 patients remained on study, all had received a minimum of 24 cycles. Sixty-six patients were evaluable for response assessment, 26 in the dose-escalation and 40 in the dose-expansion phases.

Best overall responses were 5 (8%) confirmed partial responses (PR), 34 (52%) stable disease (SD) including 1 unconfirmed partial response, and 27 (41%) progressive disease, including clinical progression (Fig. 3A-C). Of those with SD or better, 25/39 (68%) had duration on study of at least 4 months, with many showing a slowing of tumor growth (Supp. Fig. 4). For those taking 160 mg BD or more, 4/49 (8%) had PR, 30 (61%) SD and 15 (30%) PD.

Patients with RECIST PR were dosed at 40, 240 (continuous schedule), and 160 (intermittent schedule) mg BD. Median duration of response was 46.7 weeks (interquartile range: 14.9 - 251.0). Responding histologies were:

- ovarian clear cell carcinoma with *ARID1A* mutation and high mutational load (160mg BD, remains on study, 251 weeks at data cut-off, Fig. 3D, supp table 4),
- HNSCC with *CDKN2A* and *MRE11A* frameshift (160 mg BD, 170 weeks, remains on study, Fig. 3E),
- esophageal squamous cell carcinoma with HR/Fanconi pathway deficiency due to *BRIP1* frameshift mutation and *PALB2* deletion (160 mg BD, 47 weeks, Fig. 3F),

moderate mutational load (12.4 mutations/Mb) and APOBEC mutational signature (23) (24, 25)

- nasopharyngeal carcinoma with *NRAS* activating mutation (240 mg BD, 14 weeks, Fig. 3G), and
- HNSCC with *APC* frameshift and *TP53* mutation (40 mg BD, 15 weeks, Fig. 3H).

One participant had an unconfirmed PR: *TP53* mutant pancreatic adenocarcinoma with no other mutation (160 mg BD, 15 weeks, Fig. 3I)

Patients with durable RECIST SD included HNSCC with *ARID2* frameshift (99 weeks), HNSCC with no sequencing available (48 weeks), HNSCC with *CCND1* amplification (49 weeks) and digital papillary adenocarcinoma with *TP53* mutation (51 weeks).

Genomic and molecular correlates

Sequencing data were available for 5/26 patients in the dose-escalation and 36/41 in dose-expansion phases.

Patients with durable responses all had an alteration which may sensitize to ATRi (Supp. Table 3, Supp. Fig 5, Supp Fig. 6**).** For patients dosed at 40 mg BD or more, out of 11 patients with no mutation of interest, 1 had a PR (9%) and out of 30 with a mutation of interest, 4 had PR (13%). Of those with PR or SD, median duration of response was 105 days for those without a mutation of interest and 185.5 days for those with a mutation of interest.

Unless otherwise stated, participants were taking 160 mg BD, intermittent ceralasertib.

Durable responses in tumors with SWI/SNF loss

The most durable response was in a patient with clear cell ovarian carcinoma and an *ARID1A* mutation (*E21763fsX*) with loss of protein expression (Fig. 3D, Fig 3J). Seven participants had aberrations in the SWI/SNF pathway, of whom 6 derived clinical benefit. One other patient had a clear ARID1A loss on IHC: a patient with eccrine adenocarcinoma with *ARID1A* stop-gain mutation (*R693X,* resulting in truncated protein expression) and H-score 0 (Fig. 3K), with *CDKN2A* deletion (240 mg BD; SD 34 weeks). A patient with an *ARID2* frameshift-bearing HNSCC had tumor shrinkage of 29% and remains on study after 99 weeks.

Other SWI/SNF aberrations are described in supp. table 4. Notably, all other *ARID1A* mutants had high protein expression (Fig. 3L, M, N), and the responding patient also had a high TMB; there was no clear difference in TMB between patients with or without clinical benefit (Supp Fig 7).

ATM pathway

There was no relationship between ATM expression and response, or duration on study (Fig. 3A). Twenty patients had ATM protein assessed: four were defined as ATM-low, with ≤25% ATM nuclear positivity (10, 10, 5 and 0 % (fig. 3O)). Out of these, median duration on treatment was 13 weeks (range 8-29) with 3/4 experiencing SD and 1 PD.

One patient had a pathogenic *ATM* mutation (*R1898fsX*) with some protein expression (50% nuclear positive) and a co-existing *ARID1A* mutation (see above), remaining on-study for 39 weeks with SD. Another had *MRE11* stop-gain mutation (R633X), together with *CDKN2A* stop-gain, and remains on study after more than 32 months with a confirmed PR (Fig. 3E). MRE11, a component of the MRN complex, activates ATM after DNA damage.

Other aberrations

Oncogene amplification

We identified 11 patients with oncogene-driven tumors (5 *NRAS*, 2 *HRAS*, 1 *KRAS* activation, 2 *CCNE1* amplification, 1 *CCND1* amplification), of whom 3 derived clinical benefit (Supp. Fig. 5). Of those with *CCNE1* amplification, one (peritoneal carcinoma, 20 mg BD, Fig. 3Q) had a best response of PD, one (serous endometrial carcinoma, Fig. 3R) SD, on study for 12 weeks, two others had increased Cyclin E1 expression by IHC without gene amplification: serous endometrial carcinoma (Fig. 3S, with germline *BRCA1* mutation) and cervical adenocarcinoma (Fig. 3P), both with SD for 16 and 29 weeks, respectively.

P53

We have previously demonstrated no relationship between p53 functionality and ATRi sensitivity in a panel of cell lines (4). This was confirmed by the lack of difference in clinical benefit and duration on study between p53 wild-type and -mutant/-deleted tumors (Supp. Fig 6).

ATRi modulates the tumor-immune microenvironment

We have previously shown preclinically that ATRi can affect the immune tumor microenvironment (TME), particularly when combined with radiotherapy (6, 26). In support of this, paired biopsies from a responding patient (40 mg BD, HNSCC, RECIST PR) showed an increase in immune cell infiltration and PD-L1 staining on immune cells at 2 weeks (Fig. 4A).

Therefore, we profiled, in detail, the immune response to ATRi in the peripheral blood of 8 participants (best responses of 5 SD, 2 PD and 1 non-evaluable (NE), all treated with 160 mg BD intermittent schedule) and in paired tumor biopsies (on-treatment versus baseline) from 8

participants (5 SD, 2 PD and 1 NE). In the peripheral blood, we observed a reduction in regulatory T-cells (T_{regs}) and a trend towards increased CD8 T-cells, leading to an increased CD8:Treg ratio after ATRi (Fig. 4B). All were on an intermittent schedule, allowing assessment of changes after 2 weeks ceralasertib (day 14) and a 2-week break (day 29). Proportions of T-cell subsets changed after ATRi, with increased naïve and central memory CD8 and CD4 T-cells after ATRi (Fig. 4C). Importantly, there were increased frequencies of memory CD4-T_{EMRA} (effector memory re-expressing CD45RA) cells at day 29 (Fig. 4D). Detailed profiling revealed: a reduction in PD-1-positive CD8 T-cells; and NK cell activation, with a trend towards increased NKG2A- and CD69-positive NK cells with ceralasertib, which normalized after the 2-week break (Fig. 4E). The circulating myeloid compartment was also altered by ATRi, with a reduction in classical and intermediate monocytes, and a change in circulating myeloid-derived suppressor cells (MDSC), with increased granulocytic (gMDSC) and reduced monocytic (mMDSC) after ceralasertib, again trending to baseline after treatment break (Fig. 4F). Circulating cytokine levels were modulated on ceralasertib therapy, with an increase in CCL2 and decrease in CCL4 and CCL5 levels observed after 2 weeks of treatment (Fig. 4G).

Responders to ATRi have inflamed tumors

RNA sequencing of paired tumor biopsies was performed to assess differential gene expression after 2 weeks of ceralasertib treatment. Eight paired tumor biopsies were analyzed from 3 patients with PR, 4 with SD and one NE, treated at various dose levels. Additional baseline samples were also available for 1 PR and 1 SD. When all samples were considered together, there were few differences in differential gene expression between baseline and on-treatment biopsies (Fig 5A). However, when responders (PR) were compared with non-responders (SD), there were marked differences in both baseline and on-treatment gene expression (Fig. 5B, C, D, E) with clustering of a number of differentially-expressed genes according to response (Supp

Fig. 8). The most common genes that were differentially expressed were immune-related, with adaptive, innate, and cytokine-related genes highly represented (Fig. 5E). Pathway analysis of the most differentially expressed genes found that these were predominantly immune-related (Supp Fig 9). Gene-set enrichment analysis revealed enrichment of inflammatory response genes between baseline and on-treatment samples. When responders were compared to non-responders, responding patients had more inflamed tumors both at baseline and on-treatment, with significantly higher transcript levels for multiple immune-related genes (Fig. 5F). Expression of cell-type-specific genes was different between responders and non-responders. Responders had a significantly higher expression of *PTPRC* (CD45) at baseline and on-treatment than non-responders, they also had an increase in *ITGAX* (CD11c) with treatment. Several other genes showed similar elevation in responders compared with non-responders, but did not reach statistical significance (Fig. 5G). When gene expression data were used for cell-type deconvolution, some differences were observed with treatment, particularly in neutrophil and macrophage populations (Supp Fig. 10).

Baseline expression of macrophage, antigen-processing and cytokine-related genes was generally higher in responding tumors (Fig. 6A, B, C), with clustering by response. T- and NK-cell signatures were increased in responders (Supp Fig. 11A, B). When on-treatment biopsies were analyzed, there was clustering of responders in cytotoxicity (Fig. 6D), as well as cytokine and T-cell signatures (Supp Fig. 11C, D). When plotted together, baseline and on-treatment samples tended to cluster by patient, rather than by treatment, indicating a strong effect of baseline tumor inflammation on response. However, interferon-stimulated genes did appear to be upregulated in both baseline and on-treatment biopsies in responders (Supp. Fig. 12).

We counted stromal tumor-infiltrating lymphocytes (TIL) in H&E-stained sections at baseline, and for 4 paired samples (Fig. 6E). Those patients who derived clinical benefit from ceralasertib, defined as PR or greater than 16 weeks on study, had a trend to higher numbers of TIL than those who did not (Fig. 6F). Stromal TIL appeared to increase in a responding patient, but not in 3 non-responders (Fig. 6E, G).

Discussion

Our study is the largest to date of ATRi monotherapy. We have shown that ceralasertib monotherapy is tolerable, with predominantly hematological toxicities reduced by an intermittent schedule. Ceralasertib has predictable PK, plasma levels at the RP2D compare favorably with observed preclinical monotherapy IC_{50} values (ATR IC_{90} of 0.666 μM and GI_{50} of approximately 1 μM, comparable to between 270-420 ng/mL (4)(22)). We have shown target modulation in tumor tissue, and increased DNA damage in surrogate tissues. We found durable clinical benefit in diverse tumor types, with evidence suggesting multiple potential biomarkers of response to ATRi, including loss of ARID1A, genomic instability, ATM-G1 pathway abnormalities, and high tumor inflammation. Conversely, we did not find clear signals that oncogene drivers sensitize to ATRi.

Other published studies of ATRi have demonstrated similar, predominantly hematological, toxicities (27). ATRi have been combined with carboplatin (27) and with paclitaxel (28) in early phase studies. The only previously published ATRi monotherapy study of BAY1895344 also found durable responses in DDR-defective tumors – 4/11 patients with ATM protein loss or deleterious mutation, one with BRCA1 mutation had prolonged SD (29). We identified several patients with ATM loss, all without objective responses. Responses were associated with other factors involved in G1 cell cycle checkpoint control, including *MRE11*: loss will result in defective ATM activation, and a previous Chk1 inhibitor study observed a durable response associated with loss of another component of this complex (30).

Alternative ATRi are administered intravenously, the duration of enzyme inhibition may differ between these two modes of administration. This may result in differential effects on efficacy and immunomodulation. As well as convenience, oral administration with an intermittent

schedule allows bone marrow recovery between dosing periods and may allow more effective tailoring of dose exposure. The introduction of a modified schedule after emergence of toxicity outside the DLT window highlights a limitation of the 3+3 study design, and alternative designs may have been able to integrate such toxicities into dose escalation decisions. Differences in efficacy between continuous, lower-dose and intermittent, higher-dose regimens should be examined in future studies.

ARID1A is a critical component of the SWI/SNF chromatin remodeling complex, which modulates the accessibility of DNA to transcription and repair machinery, and is frequently mutated in cancers (31). ARID1A is important for ATR activation after double-stranded DNA breaks (32); it helps topoisomerase-II prevent DNA tangling during mitosis (decatenation) (33). Without this activity, cells activate a G2/M decatenation checkpoint (34). This is abolished by ATRi, leading to massive DNA damage (10). There are 2 main protein complexes in the SWI/SNF family: ARID1A, a critical component of the cBAF complex; PBRM1 and ARID2 are components of the PBAF complex (35). Only ARID1A loss has been described preclinically as an ATRi sensitizer (10), but distinct functions of different SWI/SNF complexes are unclear (35). ARID1A loss is particularly common in ovarian clear cell and uterine carcinomas (36), of 2 patients with protein loss, one responded and one had SD, suggesting other factors may also be involved. Durable responses have been reported patients with ARID1A loss in ongoing clinical studies (37, 38). Other components, such as ARID2, may also be associated with clinical benefit, as suggested by the durable SD in a participant with *ARID2* loss.

Intriguingly, ceralasertib responders in this study had more inflamed tumors at baseline. We saw ATRi-induced changes in the immune TME. Prior studies have found that ATRi can cause marked modulation of the TME, thought to be secondary to increased DNA damage and

activation of cytoplasmic DNA sensing machinery (6-8). Here, we have confirmed that treatment with ceralasertib modulates the immune response, with a more favorable CD8:T_{reg} ratio, activation of NK cells, increased frequencies of effector memory RA CD4 T cells and modulation of cytokines and circulating MDSC, as well as increase in TILs and inflammatory gene expression in responding patients. A recently published combination study of ceralasertib and immune checkpoint blockade with durvalumab in advanced gastric cancer found a benefit in those patients with ATM loss or HR deficiency and found that responders had changes in their immune TME (39). However, the specific contribution of ATRi cannot be determined from those data. Our study of ATRi monotherapy allows a unique opportunity to observe the immunomodulatory effects of these agents without immunotherapies and provides the first data that ATRi (and other DDR inhibitors) may modulate the immune TME in their own right.

The possibility that inflamed tumors may respond better to ATRi suggests that: (i) these tumors have pre-existing DDR defects which make them more inflamed and more likely to respond to ATRi (40), with the inflammation being an independent phenomenon to the response to ATRi; and/or (ii) there is modulation of anti-tumor immunity by the administration of ATRi. Although we noted that there may be increased TILs in the tumors of patients who benefitted from ATRi, the difference was modest and more substantial changes were seen between responders and non-responders on the gene expression level. Notably, ATRi seem to increase responses to immune checkpoint blockade (ICB) in patients who have previously failed ICB alone (41), adding further weight to our hypothesis that ATRi have independent immunomodulatory effects. We suggest immune analyses in ongoing ATRi studies focusing on both baseline immune status and changes with therapy to uncover rational immunotherapy partners for ATRi. In particular, the effect we have observed on NK and myeloid cells should be further investigated, particularly in light of preclinical data suggesting NK cells may have a role ATRi responses (26).

The results from this study provide the first evidence that ceralasertib monotherapy is tolerable, with antitumor activity in a number of genetic backgrounds. We have recommended a 160 mg BD two-week-on, two-week-off dosing schedule for further evaluation. Phase I-III studies are proceeding as monotherapy or in combination with PARP inhibitors in advanced solid tumors (NCT02264678), *ATM*- or *ARID1A*-mutant tumors (42) (NCT03682289), DDR-deficient tumors (NCT03462342), and in combination with immune checkpoint blockade (43, 44) (NCT02664935, NCT05061134, NCT05450692). Tumor inflammation, ARID1A loss and genome instability are among the most promising areas for future study.

Patients and Methods

Patient Population

Patients were 18 years and over, with advanced solid malignancy, without standard anti-cancer treatment options. All had ECOG performance status 0-1, life expectancy of at least 3 months and adequate organ function. Key inclusion criteria are provided in the supplementary data.

Study Design

This was a multi-part, multi-center, open-label phase I study. Part A comprised a dose escalation and part B dose expansion. During dose expansion, participants were selected based on the presence or absence of putative biomarkers of response to ATRi. Part C (combination with radiotherapy) will be reported separately. Patients in this study started ceralasertib between July 2014 and October 2020. The data cutoff was in October 2022, when 4 patients were still on study medication, all for at least 2 years.

The primary objective was to determine the safety and feasibility of administration of ceralasertib monotherapy in patients with advanced solid tumors. The secondary objectives were to identify a dose and schedule for further studies of ceralasertib and to assess anti-tumor responses and PK. Exploratory objectives included pharmacodynamic studies in tumor and normal tissue and the potential value of putative markers of sensitivity to single-agent ATRi, including measures of immune activation.

Study Treatments

Ceralasertib was administered orally, twice daily.

Part A (dose escalation, Fig 1A, 1B): The starting dose of 20 mg was selected based on animal toxicity studies. Dosing was continuous, and escalation used a modified Fibonacci method. Initial dose escalation was planned in single patient cohorts, changing to 3+3 design after the first grade 2 toxicity was seen. This occurred in the first patient. Cohorts of 3-6 patients were assessed for toxicity during a dose-limiting toxicity (DLT) window of 28 days (1 cycle), with a non-tolerable dose defined as ≥ 2/6 patients experiencing a DLT. DLT definitions are in the supplementary material.

Part B: All patients received the recommended phase 2 dose (RP2D) as defined in part A. Part B allowed for different schedules (continuous/intermittent) to be assessed. Initially, a continuous dosing schedule was used for the first 6 patients. Subsequently, the safety review committee authorized the assessment of an intermittent schedule, 14-days-on and 14-days-off. Pre-treatment biopsy was mandatory in part B. DNA sequencing of archival tumor material or review of external tumor sequencing was used to enrich for patients with putative genomic markers of sensitivity to ATRi, based on preclinical data, including: oncogene amplification or

driver mutation; ATM-G1 pathway defects (alteration in ATM, checkpoint kinase 2 (CHK2), or other components of the pathway causing G1 cell-cycle arrest after DNA damage) defect; SWI/SNF (switch/sucrose non-fermentable, a chromatin remodeling complex) pathway defect, genomic instability/homologous recombination deficit (HRD); or defect in a gene synthetically lethal with ATRi in published data (45, 46) (Fig. 1B, Supp. Table 3).

Study Assessments

Patients were assessed weekly during cycle 1 and 2-weekly thereafter, with safety assessments including blood hematology and biochemistry, physical examination and toxicity scoring. Safety and tolerability were assessed using Common Terminology Criteria for Adverse Events (CTCAE) version 4.03. Participants had ECG and urinalysis at the start of each cycle of treatment, and assessment of left ventricular ejection fraction every 8 weeks. Response assessment imaging was conducted according to RECIST 1.1, within 28 days of starting ceralasertib and every 8 weeks.

Pharmacokinetics

Intensive PK sampling in part A occurred after a single dose from pre-dose up to 24-72 hours and again at day 15 and day 29 of continuous dosing. Participants fasted for 1 h before and 2 h after dosing for PK assessment. In part B, sampling coincided with day 15 pharmacodynamic assessments. Full details are given in supplementary methods.

Pharmacodynamics and histology

PD sampling took place at baseline (within 7 days prior to dosing), and between day 15-22 of dosing (day 14 for intermittent dosing cohorts). PD samples included PBMC and tumor biopsies. PBMCs were analyzed by immunofluorescence for $\gamma^{(S139)}$H2AX, phospho-$^{(S345)}$Chk1

and total Chk1 as described in supplementary methods. Paired tumor biopsies were formalin-fixed and analyzed for nuclear phospho-$^{(S635)}$Rad50 and γH2AX by immunohistochemistry (IHC).

Translational methods

DNA sequencing of tumor and matched buffy coats was either by whole exome sequencing or a custom-designed panel targeting all exons of genes of interest for 173 genes, including potential markers of sensitivity to ATRi. ACK-lysed whole blood or PBMC were stained for flow cytometry using 8 multicolor panels. Plasma cytokines were assessed using the Bio-Plex Pro 27-plex panel (Bio-Rad). See supplementary methods for full information.

Statistical Analysis

Simple descriptive statistical data analysis methods were used to summarize the data. Categorical data using numbers and percentages of patients in the categories/groups, where appropriate 95% confidence intervals were reported. Continuous non-normally distributed data as assessed by visual inspection were described using median, interquartile range and minimum and maximum values. Statistical analyses were conducted using STATA version 17.0. Additional genomic and laboratory data were plotted and analyzed using Prism 8 (GraphPad), and ggplot2 in R version 4. For comparison of biomarkers at baseline and on-treatment, paired t-tests (two tailed) or their non-parametric equivalents were used. When comparing fold-change data normalized to baseline, Wilcoxon signed rank test with a hypothetical median of 1 (no change from baseline) was used unless otherwise stated.

Study Approval

This study was conducted in accordance with protocol requirements, Good Clinical Practice (GCP) and the Declaration of Helsinki. All participants provided written informed consent. The protocol was approved by the local ethics committee (NRES Committee London - City and East, reference 14/LO/0465).

Data availability

Individual participant data that underlie the figures in this article will be made available, upon de-identification, to researchers who provide a methodologically sound proposal. Requests should be submitted to magnus.dillon@icr.ac.uk, a signed data access agreement will be required. Tumor profiling, flow cytometry and clinical annotations can be provided. Pharmacokinetic and pharmacodynamic data will not be provided.

List of supplementary materials:

Supplementary materials and methods

Supplementary data (individual values used to present average data in main figures)

Fig. S1-13

Table S1-4

Author contributions:

Study conceptualization, design and protocol writing was by MTD, SAS, MDF and KJH.

Study safety review was by KJH, UB, MS, JS, MDF, KJH.

JG was the study manager, KM the statistician.

PP and KES were responsible for genomic and pharmacodynamic assessments.

IHC staining and analysis was supported by GNH, SW, KT, LM, PM, IR, AW. PK analysis was performed by MP and CS.

Immune assays and analysis were performed by EP and MM.

Authors contributing through participant support, site-level investigation were MTD, JG, ECP, GNJ, SEW, MP, CS, KT, IR, PN, AW, MM, AJL, SB, GN, VK, LG, SM, PP, PM, LM, SK, JS, MDF and KJH

The original draft of the manuscript was written by MTD, KM, KJH and reviewed and edited by MTD, JG, KM, ECP, SAS, ED, GNJ, MP, CS, CB, PN, AW, PP, KS, UB, MS, JS, MDF and KJH. All authors approved the final manuscript.

Acknowledgements:

We would like to thank The Breast Cancer Now histopathology core facility and the Institute of Cancer Research Genomics Facility. We acknowledge Dr Magnus Hallin and Dr Martine Roudier for pathology support and assistance with scoring IHC slides. We would like to thank Michael Hubank, Clinical Genomics at RMH for assistance with panel design and validation and the ICR genomics facility, Anton Patrikeev and Ritika Chauhan for bioinformatic analysis.

This study was co-sponsored by The Royal Marsden and The Institute of Cancer Research. Financial and drug support was provided by AstraZeneca and Cancer Research UK, through the CRUK Combinations Alliance. The authors acknowledge additional financial support from the UK Department of Health and Cancer Research UK via Experimental Cancer Medicine Centre and NIHR Biomedical Research Centre grants to Institute of Cancer Research/Royal Marsden Hospital, King's Health Partners/Guy's & St Thomas' NHS Foundation Trust, and University College London/UCL Hospital NHS Trust. This project represents independent research supported by the National Institute for Health and Care Research (NIHR). The views

expressed are those of the authors and not necessarily those of the NIHR or the Department of Health and Social Care.

Funding:

Cancer Research UK C7224/A23275, CRUKD/14/007 (KJH)

Cancer Research UK C347/A18077, C309/A25144, CTRQQR-2021\100009 (KS)

Cancer Research UK (MTD)

AstraZeneca

UK Department of Health (National Institute for Health Research) NIHR202438 (KJH)

UK Department of Health (National Institute for Health Research) (MTD, MDF)

Rosetrees Trust (KJH, MTD)

CRIS Cancer Foundation (PN)

Experimental Cancer Medicine Centre

Competing Interests:

KES is an employee of The Institute of Cancer Research, which is involved in the development of PI3K, HSP90, HDAC, AKT, ROCK, RAF, CHK1 and HSF1 inhibitors.

UB reports research funding, honoraria and advisory board membership for Chugai Pharmaceutical, Verastem Inc., and Carrick Therapeutics

JS reports stock ownership: Epsilogen Ltd; Research funding (inst.) Achilles, BergenBio, Gilead, GSK, IO Biotech, MSD, Roche, RS Oncology, SeaGen, Starpharma; Advisory roles (inst.): 4D Pharma, Apobec, Avacta, AstraZeneca, BMS, Roche; Meeting assistance: BMS, MSD.

KJH reports honoraria (inst.): Arch Oncology, AstraZeneca, BMS, Boehringer Ingelheim, Codiak Biosciences, F-Star Therapeutics, Inzen Therapeutics, Merck Serono, MSD, Oncolys Biopharma, Pfizer, Replimune, VacV Biotherapeutics; Consulting or Advisory Role (inst.): Arch Oncology, AstraZeneca, BMS, Boehringer Ingelheim, Inzen Therapeutics, Merck Serono, MSD,

Oncolys BioPharma, Replimune; Speakers' Bureau (inst.): BMS, Merck Serono, MSD; Research Funding (inst.): AstraZeneca, Boehringer Ingelheim, Merck Sharp & Dohme, Replimune.

GJ, SW, MP, CS, PM, LM, SAS, ED are employees of AstraZeneca with stock ownership.

Clinical trial information

Clinicaltrials.gov: NCT02223923

EudraCT: 2013-003994-84

References

1. Bradbury A, Hall S, Curtin N, and Drew Y. Targeting ATR as Cancer Therapy: A new era for synthetic lethality and synergistic combinations? *Pharmacology & therapeutics.* 2020;207:107450.
2. Cimprich KA, and Cortez D. ATR: an essential regulator of genome integrity. *Nature reviews Molecular cell biology.* 2008;9(8):616-27.
3. Lecona E, and Fernandez-Capetillo O. Targeting ATR in cancer. *Nature reviews Cancer.* 2018.
4. Dillon MT, Barker HE, Pedersen M, Hafsi H, Bhide SA, Newbold KL, et al. Radiosensitization by the ATR Inhibitor AZD6738 through Generation of Acentric Micronuclei. *Molecular cancer therapeutics.* 2017;16(1):25-34.
5. Lau A, Brown E, Thomason A, Odedra R, Sheridan V, Cadogan E, et al. Abstract C60: Pre-clinical efficacy of the ATR inhibitor AZD6738 in combination with the PARP inhibitor olaparib. *Molecular cancer therapeutics.* 2015;14(12 Supplement 2):C60-C.
6. Dillon MT, Bergerhoff KF, Pedersen M, Whittock H, Crespo-Rodriguez E, Patin EC, et al. ATR Inhibition Potentiates the Radiation-induced Inflammatory Tumor Microenvironment. *Clinical cancer research : an official journal of the American Association for Cancer Research.* 2019;25(11):3392-403.
7. Feng X, Tubbs A, Zhang C, Tang M, Sridharan S, Wang C, et al. ATR inhibition potentiates ionizing radiation-induced interferon response via cytosolic nucleic acid-sensing pathways. *The EMBO journal.* 2020:e104036.
8. Vendetti FP, Karukonda P, Clump DA, Teo T, Lalonde R, Nugent K, et al. ATR kinase inhibitor AZD6738 potentiates CD8+ T cell-dependent antitumor activity following radiation. *The Journal of clinical investigation.* 2018;128(9):3926-40.
9. Kwok M, Davies N, Agathanggelou A, Smith E, Oldreive C, Petermann E, et al. ATR inhibition induces synthetic lethality and overcomes chemoresistance in TP53- or ATM-defective chronic lymphocytic leukemia cells. *Blood.* 2016;127(5):582-95.
10. Williamson CT, Miller R, Pemberton HN, Jones SE, Campbell J, Konde A, et al. ATR inhibitors as a synthetic lethal therapy for tumours deficient in ARID1A. *Nature Communications.* 2016;7:13837.
11. Middleton FK, Patterson MJ, Elstob CJ, Fordham S, Herriott A, Wade MA, et al. Common cancer-associated imbalances in the DNA damage response confer sensitivity to single agent ATR inhibition. *Oncotarget.* 2015;6(32):32396-409.
12. Mohni KN, Kavanaugh GM, and Cortez D. ATR pathway inhibition is synthetically lethal in cancer cells with ERCC1 deficiency. *Cancer research.* 2014;74(10):2835-45.
13. Sultana R, Abdel-Fatah T, Perry C, Moseley P, Albarakti N, Mohan V, et al. Ataxia Telangiectasia Mutated and Rad3 Related (ATR) Protein Kinase Inhibition Is Synthetically Lethal in XRCC1 Deficient Ovarian Cancer Cells. *PloS one.* 2013;8(2):e57098.
14. Toledo LI, Murga M, Zur R, Soria R, Rodriguez A, Martinez S, et al. A cell-based screen identifies ATR inhibitors with synthetic lethal properties for cancer-associated mutations. *Nature structural & molecular biology.* 2011;18(6):721-7.
15. Murga M, Campaner S, Lopez-Contreras AJ, Toledo LI, Soria R, Montana MF, et al. Exploiting oncogene-induced replicative stress for the selective killing of Myc-driven tumors. *Nature structural & molecular biology.* 2011;18(12):1331-5.
16. Gilad O, Nabet BY, Ragland RL, Schoppy DW, Smith KD, Durham AC, et al. Combining ATR suppression with oncogenic Ras synergistically increases genomic instability, causing synthetic lethality or tumorigenesis in a dosage-dependent manner. *Cancer research.* 2010;70(23):9693-702.

17. Medler T, Patel JM, Alice A, Baird JR, Hu HM, and Gough MJ. Activating the Nucleic Acid-Sensing Machinery for Anticancer Immunity. *Int Rev Cell Mol Biol.* 2019;344:173-214.
18. Foote KM, Nissink JWM, McGuire T, Turner P, Guichard S, Yates JWT, et al. Discovery and Characterization of AZD6738, a Potent Inhibitor of Ataxia Telangiectasia Mutated and Rad3 Related (ATR) Kinase with Application as an Anticancer Agent. *Journal of medicinal chemistry.* 2018;61(22):9889-907.
19. Guichard SM, Brown E, Odedra R, Hughes A, Heathcote D, Barnes J, et al. Abstract 3343: The pre-clinical in vitro and in vivo activity of AZD6738: A potent and selective inhibitor of ATR kinase. *Cancer research.* 2013;73(8 Supplement):3343.
20. Dillon MT, Boylan Z, Smith D, Guevara J, Mohammed K, Peckitt C, et al. PATRIOT: A phase I study to assess the tolerability, safety and biological effects of a specific ataxia telangiectasia and Rad3-related (ATR) inhibitor (AZD6738) as a single agent and in combination with palliative radiation therapy in patients with solid tumours. *Clin Transl Radiat Oncol.* 2018;12:16-20.
21. Pierce A, Berges A, Cheung SYA, Standifer N, Ross G, Smith S, et al. Dose-exposure-response relationship between AZD6738 and peripheral monocytes. *Journal of Clinical Oncology.* 2017;35(15_suppl):e14063-e.
22. Wilson Z, Odedra R, Wallez Y, Wijnhoven PWG, Hughes AM, Gerrard J, et al. ATR Inhibitor AZD6738 (Ceralasertib) Exerts Antitumor Activity as a Monotherapy and in Combination with Chemotherapy and the PARP Inhibitor Olaparib. *Cancer research.* 2022;82(6):1140-52.
23. Alexandrov LB, Nik-Zainal S, Wedge DC, Aparicio SAJR, Behjati S, Biankin AV, et al. Signatures of mutational processes in human cancer. *Nature.* 2013;500(7463):415-21.
24. Green AM, Budagyan K, Hayer KE, Reed MA, Savani MR, Wertheim GB, et al. Cytosine deaminase APOBEC3A sensitizes leukemia cells to inhibition of the DNA replication checkpoint. *Cancer research.* 2017.
25. Nikkila J, Kumar R, Campbell J, Brandsma I, Pemberton HN, Wallberg F, et al. Elevated APOBEC3B expression drives a kataegic-like mutation signature and replication stress-related therapeutic vulnerabilities in p53-defective cells. *British journal of cancer.* 2017;117(1):113-23.
26. Patin EC, Dillon MT, Nenclares P, Grove L, Soliman H, Leslie I, et al. Harnessing radiotherapy-induced NK-cell activity by combining DNA damage-response inhibition and immune checkpoint blockade. *J Immunother Cancer.* 2022;10(3).
27. Yap TA, O'Carrigan B, Penney MS, Lim JS, Brown JS, de Miguel Luken MJ, et al. Phase I Trial of First-in-Class ATR Inhibitor M6620 (VX-970) as Monotherapy or in Combination With Carboplatin in Patients With Advanced Solid Tumors. *Journal of clinical oncology : official journal of the American Society of Clinical Oncology.* 2020;38(27):3195-204.
28. Lee J, Kim ST, Smith S, Mortimer PG, Loembé B, Hong J, et al. Results from a phase I, open-label study of ceralasertib (AZD6738), a novel DNA damage repair agent, in combination with weekly paclitaxel in refractory cancer (NCT02630199). *Journal of Clinical Oncology.* 2020;38(15_suppl):3503-.
29. Yap TA, Tan DS, Terbuch A, Caldwell R, Guo C, Goh BC, et al. First-in-Human Trial of the Oral Ataxia Telangiectasia and Rad3-Related Inhibitor BAY 1895344 in Patients with Advanced Solid Tumors. *Cancer discovery.* 2020.
30. Al-Ahmadie H, Iyer G, Hohl M, Asthana S, Inagaki A, Schultz N, et al. Synthetic lethality in ATM-deficient RAD50-mutant tumors underlies outlier response to cancer therapy. *Cancer discovery.* 2014;4(9):1014-21.
31. Kadoch C, Hargreaves DC, Hodges C, Elias L, Ho L, Ranish J, et al. Proteomic and bioinformatic analysis of mammalian SWI/SNF complexes identifies extensive roles in human malignancy. *Nature genetics.* 2013;45(6):592-601.

32. Shen J, Peng Y, Wei L, Zhang W, Yang L, Lan L, et al. ARID1A Deficiency Impairs the DNA Damage Checkpoint and Sensitizes Cells to PARP Inhibitors. *Cancer discovery.* 2015;5(7):752-67.
33. Dykhuizen EC, Hargreaves DC, Miller EL, Cui K, Korshunov A, Kool M, et al. BAF complexes facilitate decatenation of DNA by topoisomerase IIα. *Nature.* 2013;497(7451):624-7.
34. Downes CS, Clarke DJ, Mullinger AM, Giménez-Abián JF, Creighton AM, and Johnson RT. A topoisomerase II-dependent G2 cycle checkpoint in mammalian cells. *Nature.* 1994;372(6505):467-70.
35. Mittal P, and Roberts CWM. The SWI/SNF complex in cancer - biology, biomarkers and therapy. *Nature reviews Clinical oncology.* 2020;17(7):435-48.
36. Khalique S, Naidoo K, Attygalle AD, Kriplani D, Daley F, Lowe A, et al. Optimised ARID1A immunohistochemistry is an accurate predictor of ARID1A mutational status in gynaecological cancers. *J Pathol Clin Res.* 2018;4(3):154-66.
37. Aggarwal R, Umetsu S, Dhawan M, Grabowsky J, Carnevale J, Howell M, et al. 512O Interim results from a phase II study of the ATR inhibitor ceralasertib in ARID1A-deficient and ARID1A-intact advanced solid tumor malignancies. *Annals of Oncology.* 2021;32:S583.
38. Banerjee S, Leary A, Stewart JR, Dewan M, Lheureux S, Clamp AR, et al. 34O ATR inhibitor alone (ceralasertib) or in combination with olaparib in gynaecological cancers with ARID1A loss or no loss: Results from the ENGOT/GYN1/NCRI ATARI trial. *ESMO Open.* 2023;8(1).
39. Kwon M, Kim G, Kim R, Kim KT, Kim ST, Smith S, et al. Phase II study of ceralasertib (AZD6738) in combination with durvalumab in patients with advanced gastric cancer. *J Immunother Cancer.* 2022;10(7).
40. Mouw KW, Goldberg MS, Konstantinopoulos PA, and D'Andrea AD. DNA Damage and Repair Biomarkers of Immunotherapy Response. *Cancer discovery.* 2017;7(7):675-93.
41. Kim R, Kwon M, An M, Kim ST, Smith SA, Loembe AB, et al. Phase II study of ceralasertib (AZD6738) in combination with durvalumab in patients with advanced/metastatic melanoma who have failed prior anti-PD-1 therapy. *Annals of oncology : official journal of the European Society for Medical Oncology / ESMO.* 2022;33(2):193-203.
42. Banerjee S, Stewart J, Porta N, Toms C, Leary A, Lheureux S, et al. ATARI trial: ATR inhibitor in combination with olaparib in gynecological cancers with ARID1A loss or no loss (ENGOT/GYN1/NCRI). *Int J Gynecol Cancer.* 2021;31(11):1471-5.
43. Robert C, Lee J, Sharfman W, Larkin J, Ascierto PA, Weber J, et al. MONETTE: Phase 2 study of ceralasertib (cerala) ± durvalumab
(durva) in patients with advanced melanoma resistant to PD-(L)1
inhibition, presented at 19th International Congress of the Society for Melanoma Research. *Pigment Cell & Melanoma Research.* 2023;36(1):86-200.
44. Besse B, Awad M, Forde P, Thomas M, Park K, Goss G, et al. OA07.08 HUDSON: An Open-Label, Multi-Drug, Biomarker-Directed, Phase II Platform Study in Patients with NSCLC, who Progressed on Anti-PD(L)1 Therapy. *Journal of Thoracic Oncology.* 2021;16(3):S118-S9.
45. Hustedt N, Álvarez-Quilón A, McEwan A, Yuan JY, Cho T, Koob L, et al. A consensus set of genetic vulnerabilities to ATR inhibition. *Open Biol.* 2019;9(9):190156.
46. Dillon MT, and Harrington KJ. In: Pollard J, and Curtin NJ eds. *Targeting the DNA Damage Response for Anti-Cancer Therapy*. London: Springer; 2018:99-127.
47. *Guidance for Industry, Bioanalytical Method Validation, U.S. Department of Health
and Human Services, Food and Drug Administration, Center for Drug Evaluation
and Research (CDER), Center for Veterinary Medicine (CMV)*. Rockville, MD: Food and Drug Administration; 2018.

48. Subramanian A, Tamayo P, Mootha VK, Mukherjee S, Ebert BL, Gillette MA, et al. Gene set enrichment analysis: a knowledge-based approach for interpreting genome-wide expression profiles. *Proceedings of the National Academy of Sciences of the United States of America.* 2005;102(43):15545-50.
49. Liberzon A, Birger C, Thorvaldsdóttir H, Ghandi M, Mesirov JP, and Tamayo P. The Molecular Signatures Database (MSigDB) hallmark gene set collection. *Cell Syst.* 2015;1(6):417-25.
50. Bindea G, Mlecnik B, Tosolini M, Kirilovsky A, Waldner M, Obenauf AC, et al. Spatiotemporal dynamics of intratumoral immune cells reveal the immune landscape in human cancer. *Immunity.* 2013;39(4):782-95.
51. Newman AM, Steen CB, Liu CL, Gentles AJ, Chaudhuri AA, Scherer F, et al. Determining cell type abundance and expression from bulk tissues with digital cytometry. *Nat Biotechnol.* 2019;37(7):773-82.
52. Jones GN, Rooney C, Griffin N, Roudier M, Young LA, Garcia-Trinidad A, et al. pRAD50: a novel and clinically applicable pharmacodynamic biomarker of both ATM and ATR inhibition identified using mass spectrometry and immunohistochemistry. *British journal of cancer.* 2018.
53. Bankhead P, Loughrey MB, Fernández JA, Dombrowski Y, McArt DG, Dunne PD, et al. QuPath: Open source software for digital pathology image analysis. *Scientific Reports.* 2017;7(1):16878.
54. Schmidt U, Weigert M, Broaddus C, and Myers G. In: Frangi AF, Schnabel JA, Davatzikos C, Alberola-López C, and Fichtinger G eds. *Medical Image Computing and Computer Assisted Intervention – MICCAI 2018*. Cham: Springer International Publishing; 2018:265-73.

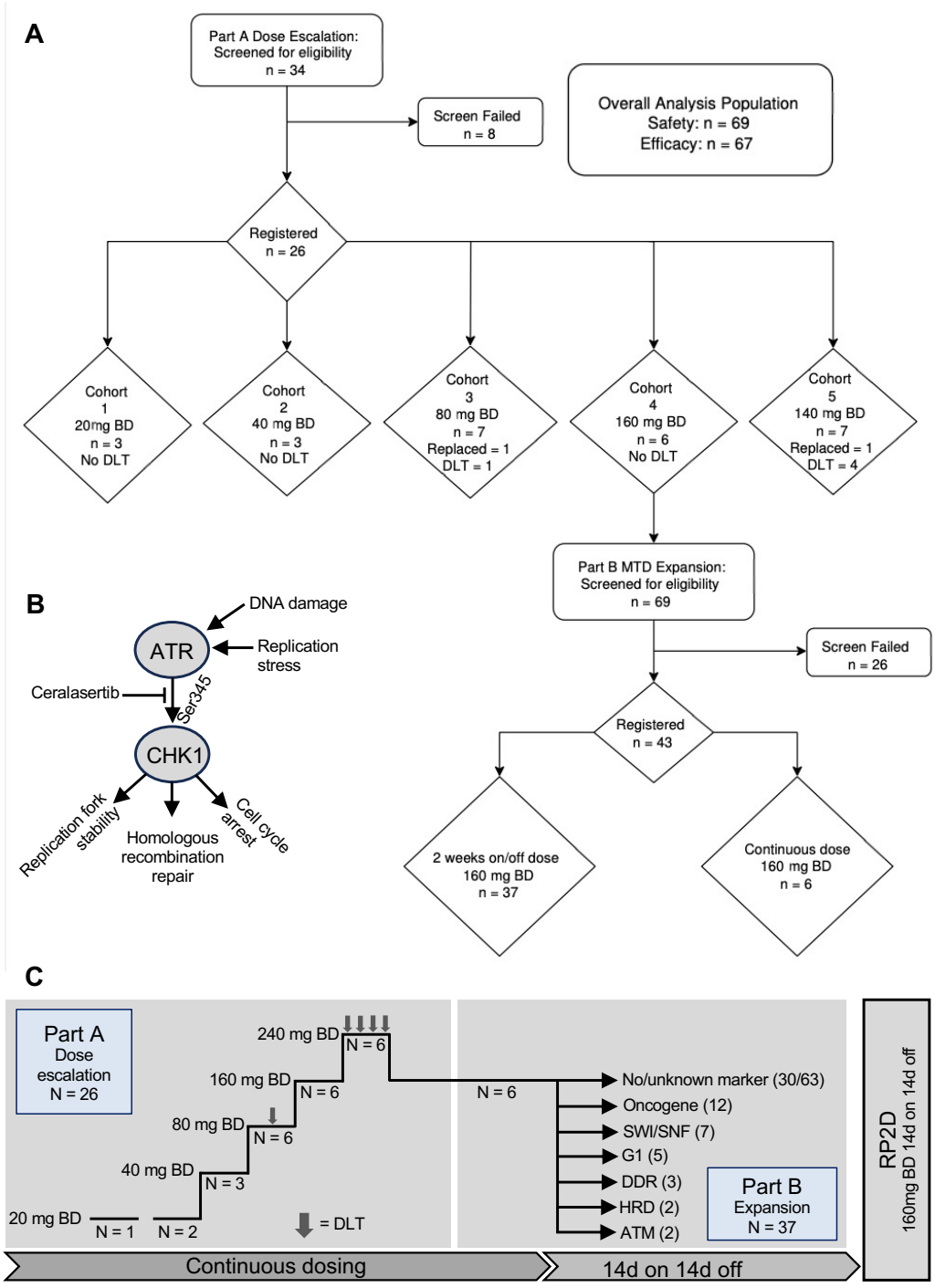
A
Part A Dose Escalation:
Screened for eligibility
n = 34
Screen Failed
n = 8
Overall Analysis Population
Safety: n = 69
Efficacy: n = 67
Registered
n = 26
Cohort
1
20mg BD
n = 3
No DLT
Cohort
2
40 mg BD
n = 3
No DLT
Cohort
3
80 mg BD
n = 7
Replaced = 1
DLT = 1
Cohort
4
160 mg BD
n = 6
No DLT
Cohort
5
140 mg BD
n = 7
Replaced = 1
DLT = 4
Part B MTD Expansion:
Screened for eligibility
n = 69
Screen Failed
n = 26
Registered
n = 43
2 weeks on/off dose
160 mg BD
n = 37
Continuous dose
160 mg BD
n = 6
B
DNA damage
ATR
Replication
stress
Ceralasertib
Ser345
CHK1
Replication fork
stability
Homologous
recombination
repair
Cell cycle
arrest
C
Part A
Dose
escalation
N = 26
240 mg BD
N = 6
160 mg BD
N = 6
80 mg BD
N = 6
40 mg BD
N = 3
20 mg BD
N = 1
N = 2
= DLT
N = 6
No/unknown marker (30/63)
Oncogene (12)
SWI/SNF (7)
G1 (5)
DDR (3)
HRD (2)
ATM (2)
Part B
Expansion
N = 37
RP2D
160mg BD 14d on 14d off
Continuous dosing
14d on 14d off

Fig 1

Figure Legends

Figure 1: Study design

A: CONSORT diagram of study parts A and B.

B: Schematic of role of ATR in DNA damage response signalling.

C: Study schema for parts A and B. In part A, all patients received continuous dosing. In part B, they received continuous or intermittent dosing. Part B patients had mandatory tumor biopsy at baseline. All patients had PD sampling (PBMC, hair follicles) at baseline and day 14-22. Response assessment was after 2 cycles of treatment.

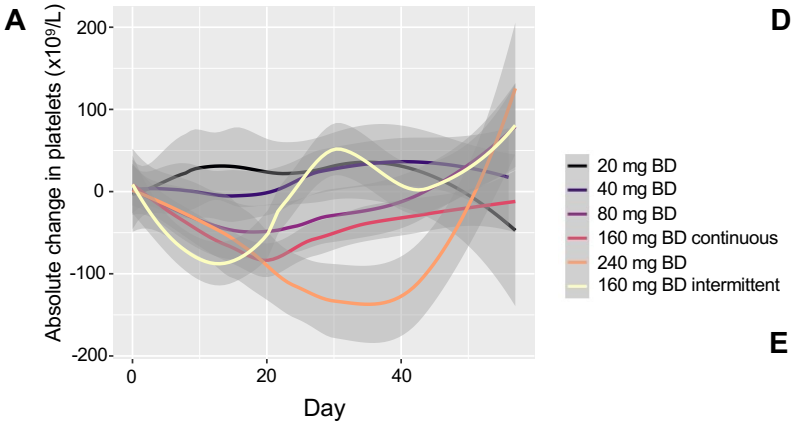
A
Absolute change in platelets (x10⁹/L)
200
100
0
-100
-200
0
20
40
Day
20 mg BD
40 mg BD
80 mg BD
160 mg BD continuous
240 mg BD
160 mg BD intermittent

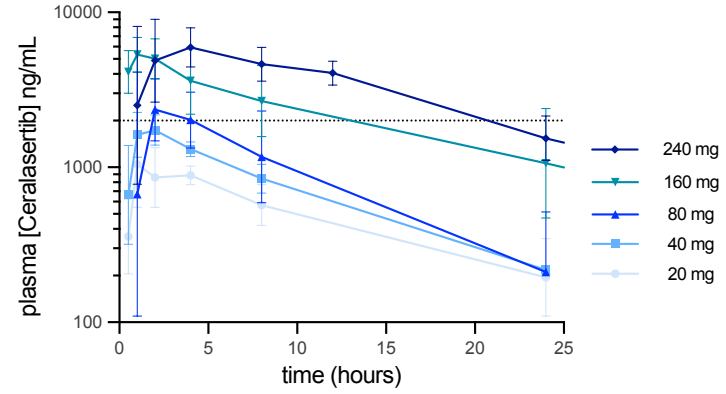
B
plasma [Ceralasertib] ng/mL
10000
1000
100
0
5
10
15
20
25
time (hours)
240 mg
160 mg
80 mg
40 mg
20 mg

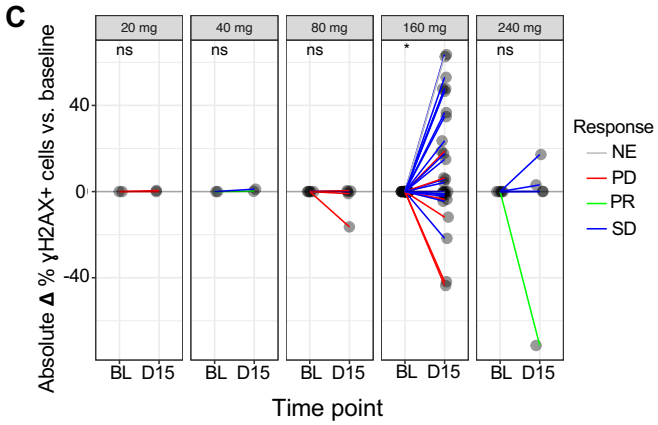
C
20 mg
40 mg
80 mg
160 mg
240 mg
ns
ns
ns
*
ns
Absolute Δ % γH2AX+ cells vs. baseline
40
0
-40
BL D15
BL D15
BL D15
BL D15
BL D15
Time point
Response
NE
PD
PR
SD

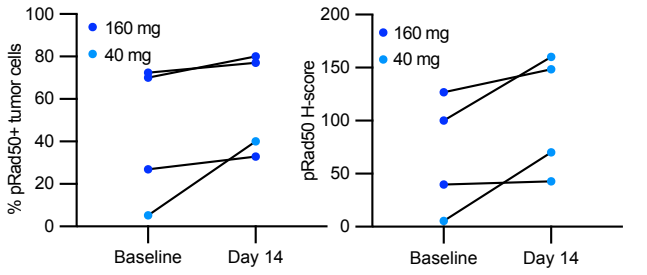
D
% pRad50+ tumor cells
100
80
60
40
20
0
160 mg
40 mg
Baseline
Day 14
pRad50 H-score
200
150
100
50
0
160 mg
40 mg
Baseline
Day 14

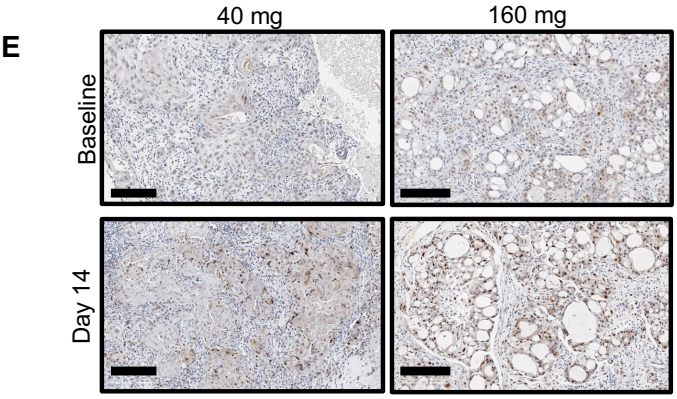
E
40 mg
160 mg
Baseline
Day 14

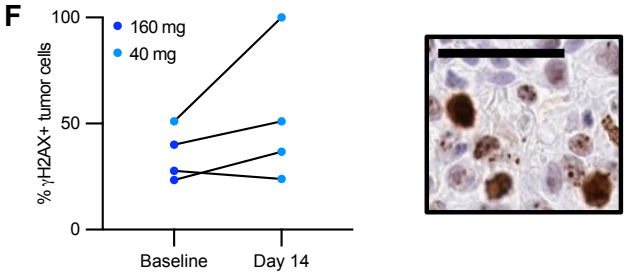
F
% γH2AX+ tumor cells
100
50
0
160 mg
40 mg
Baseline
Day 14

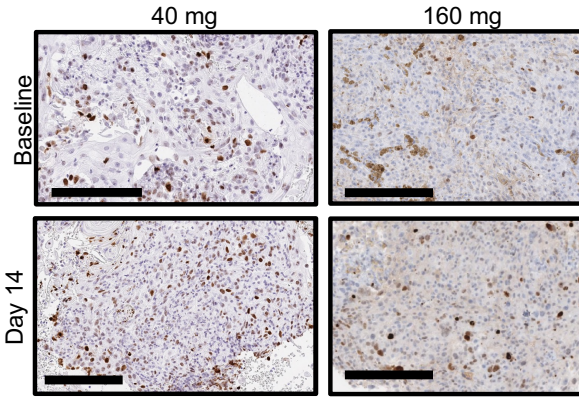
G
40 mg
160 mg
Baseline
Day 14

Fig 2

Figure 2: Pharmacokinetics and pharmacodynamics

A: Change in platelet count with time, by dose cohort. Smoothed conditional mean absolute changes compared with baseline blood count are presented, with 95% CI.

B: Ceralasertib PK. Geometric mean (and SD) plasma concentration over time after a single dose at the indicated dose levels (semi-log scale)

C: Absolute change in γH2AX-positive PBMCs (defined as percent of cells with >5 foci) after 2-week dosing at the indicated dose levels. Line color indicates RECIST response, *: p = 0.046 by Wilcoxon signed rank test with a hypothetical median of 0.

D: Tumor pharmacodynamics. Change in phospho-$^{(S635)}$Rad50 in paired tumor biopsies, after 2-week dosing. pRad50 in tumor cells expressed by % positive (left) and H-score (right), for the indicated dose levels. Fold change vs. baseline p = 0.13 by Wilcoxon signed rank test.

E: Examples of staining for pRad50 for the indicated dose levels. Scale bar: 200 μm. Left panel, HNSCC, 40 mg BD, RECIST PR. Right panel, parotid adenocarcinoma, 160 mg BD, RECIST SD.

F: Evidence of increased replication stress with ceralasertib treatment. Immunohistochemical staining for γH2AX in paired tumor biopsies. Left: change in % positive tumor cells (defined as at least 5 nuclear foci or pan-nuclear staining) after 2-week dosing, p=0.22 by paired t-test. Right: examples of nuclear foci and pan-nuclear staining after treatment, scale bar = 50 μm.

G: Examples of γH2AX staining for the indicated dose levels: left panel, HNSCC, 40 mg BD, RECIST PR. Right panel, serous ovarian carcinoma, 160 mg BD, RECIST SD.

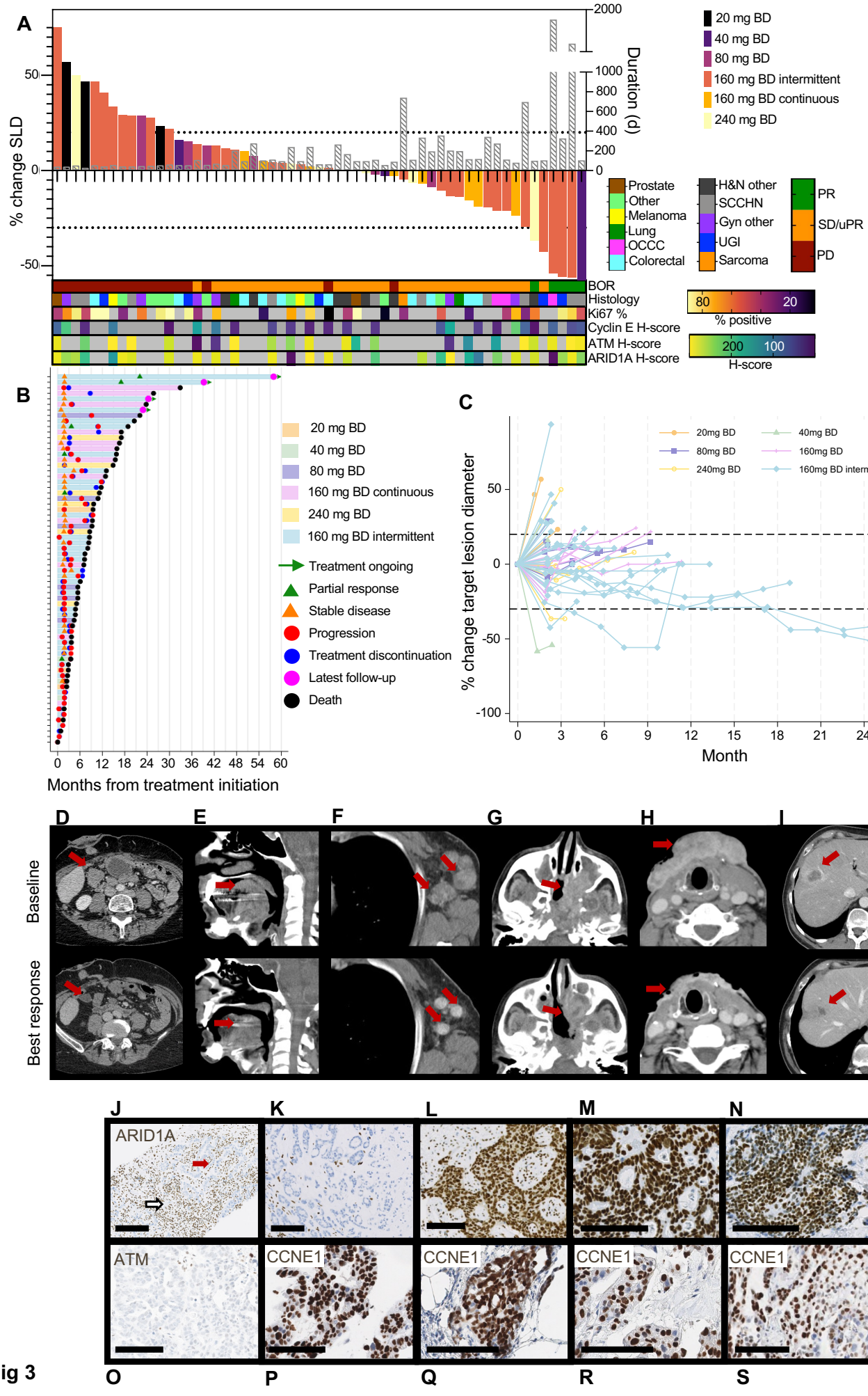
A
% change SLD
Duration (d)
20 mg BD
40 mg BD
80 mg BD
160 mg BD intermittent
160 mg BD continuous
240 mg BD
Prostate
Other
Melanoma
Lung
OCCC
Colorectal
H&N other
SCCHN
Gyn other
UGI
Sarcoma
PR
SD/uPR
PD
BOR
Histology
Ki67 %
Cyclin E H-score
ATM H-score
ARID1A H-score
% positive
H-score
B
Treatment ongoing
Partial response
Stable disease
Progression
Treatment discontinuation
Latest follow-up
Death
Months from treatment initiation
C
% change target lesion diameter
Month
20mg BD
40mg BD
80mg BD
160mg BD
240mg BD
160mg BD intermittent
D
E
F
G
H
I
Baseline
Best response
J
K
L
M
N
ARID1A
ATM
CCNE1
O
P
Q
R
S

Fig 3

Figure 3: Anti-tumor responses

A: waterfall plot of best change in sum of diameters of target lesions, with corresponding duration on study.

B: swimmer plot of evaluable patients

C: spider plot of evaluable patients

D-I: Representative scans from responding patients:

D: Ovarian clear cell carcinoma, ARID1A loss, RECIST PR, 1763 days on study, 160 mg BD intermittent

E: HNSCC, MRE11 and CDKN2A mutation, 1194 days on study

F: Esophageal squamous cell carcinoma, HR and Fanconi pathway deficiency, RECIST PR, 575 days on study, 160 mg BD intermittent

G: Nasopharyngeal carcinoma, NRAS activation, RECIST PR, 341 days on study, 240 mg BD

H: HNSCC, RECIST PR, 106 days on study, 40 mg BD.

I: Pancreatic adenocarcinoma, no clear mutation, unconfirmed PR, 480 days on study, 160 mg BD intermittent

Tumor protein profiling: IHC tumor staining was performed on the cases mentioned

J: Clear cell ovarian carcinoma with loss of ARID1A, H-score 0, red arrowhead indicates tumor cells, white indicates stroma

K: Eccrine adenocarcinoma with loss of ARID1A, H-score 0

L: Lung adenocarcinoma, ARID1A mutation but no protein loss (H-score 290)

M: Cervix adenocarcinoma, ARID1A mutation but no protein loss (H-score 300)

N: Clear cell ovarian carcinoma, ARID1A mutation but no protein loss (H-score 235)

O: Serous ovarian carcinoma, ATM protein loss.

P: Same tumor as (M), showing cyclin E1 overexpression (H-score 169)

Q: Peritoneal carcinoma, CCNE1 amplification on sequencing, cyclin E1 H-score 210

R: Serous endometrial carcinoma, CCNE1 amplification on sequencing, cyclin E1 H-score 224

S: Serous endometrial carcinoma, CCNE1 overexpression by IHC, cyclin E1 H-score 155.

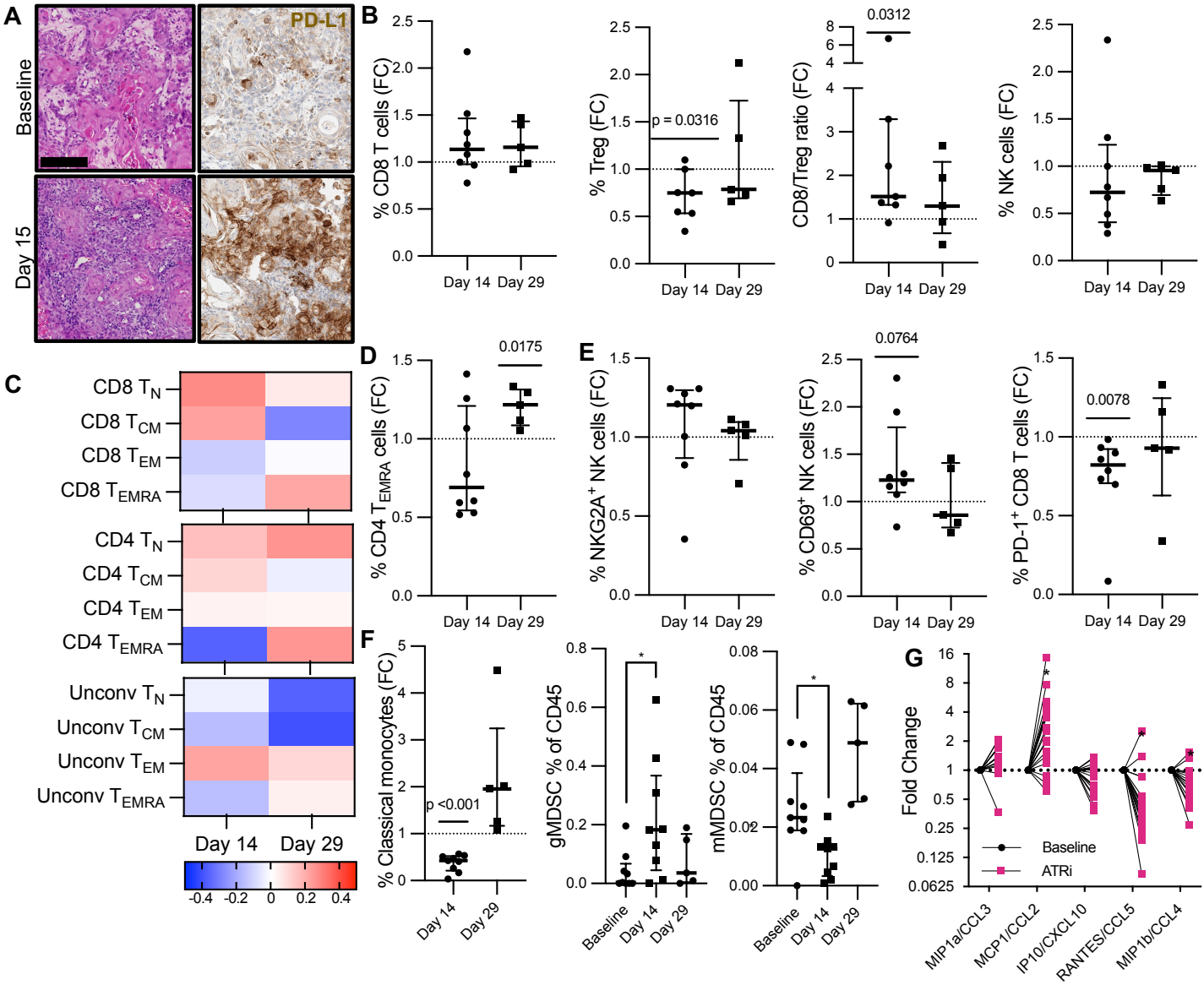
A
Baseline
Day 15
PD-L1
B
% CD8 T cells (FC)
% Treg (FC)
p = 0.0316
CD8/Treg ratio (FC)
0.0312
% NK cells (FC)
Day 14 Day 29
C
CD8 T_N
CD8 T_CM
CD8 T_EM
CD8 T_EMRA
CD4 T_N
CD4 T_CM
CD4 T_EM
CD4 T_EMRA
Unconv T_N
Unconv T_CM
Unconv T_EM
Unconv T_EMRA
Day 14 Day 29
-0.4 -0.2 0 0.2 0.4
D
% CD4 T_EMRA cells (FC)
0.0175
E
% NKG2A+ NK cells (FC)
% CD69+ NK cells (FC)
0.0764
% PD-1+ CD8 T cells (FC)
0.0078
F
% Classical monocytes (FC)
p <0.001
gMDSC % of CD45
mMDSC % of CD45
Baseline
Day 14
Day 29
G
Fold Change
Baseline
ATRi
MIP1a/CCL3
MCP1/CCL2
IP10/CXCL10
RANTES/CCL5
MIP1b/CCL4

Fig 4

Figure 4: Immune profiling

A: H&E and PD-L1 IHC staining of paired biopsies of a responding patient (HNSCC, 40 mg, RECIST PR), showing infiltration of PD-L1 positive immune cells after 2 weeks' ceralasertib. Scale bar = 200 □m.

B: Fold change in percent of CD45+ cells in peripheral blood, after two weeks' ceralasertib (day 14) and after a two-week break (day 29), compared with baseline sample for the indicated cell type. Median and interquartile range (IQR) indicated. Statistical significance by Wilcoxon test.

C: Log2 fold change in percent of the CD8+ T, CD4+ T and Unconventional T cells of the following populations TN (T naïve as CCR7+/CD45RA+), TCM (T central memory as CCR7+/CD45RA-), TEM (T effector memory as CCR7-/CD45RA-) and TEMRA (T effector memory RA as CCR7-/CD45RA+) from baseline, median and IQR indicated.

D: Fold change in percent of CD45 of memory CD4-TEMRA (effector memory re-expressing CD45RA) from baseline. Median and IQR indicated. Statistical significance by Wilcoxon test.

E: Fold change in percent of NK cells or CD8+ T cells in the peripheral blood of (from left to right) NK cell NKG2A-positive, NK cell CD69-positive and CD8+ T-cell PD1-postitive from baseline. Median and IQR indicated. Statistical significance by Wilcoxon test.

F: Left: fold change in percent of CD45 of classical monocytes, as above. Middle: change in gMDSC as a percentage of CD45-positive cells, right: change in mMDSC as a percentage of CD45-positive cells. Median and IQR indicated; *: $p<0.05$ by unpaired t-test.

G: fold change vs baseline in levels of the indicated plasma cytokines, after 2 weeks' ceralasertib. * $p< 0.05$ by paired t-test.

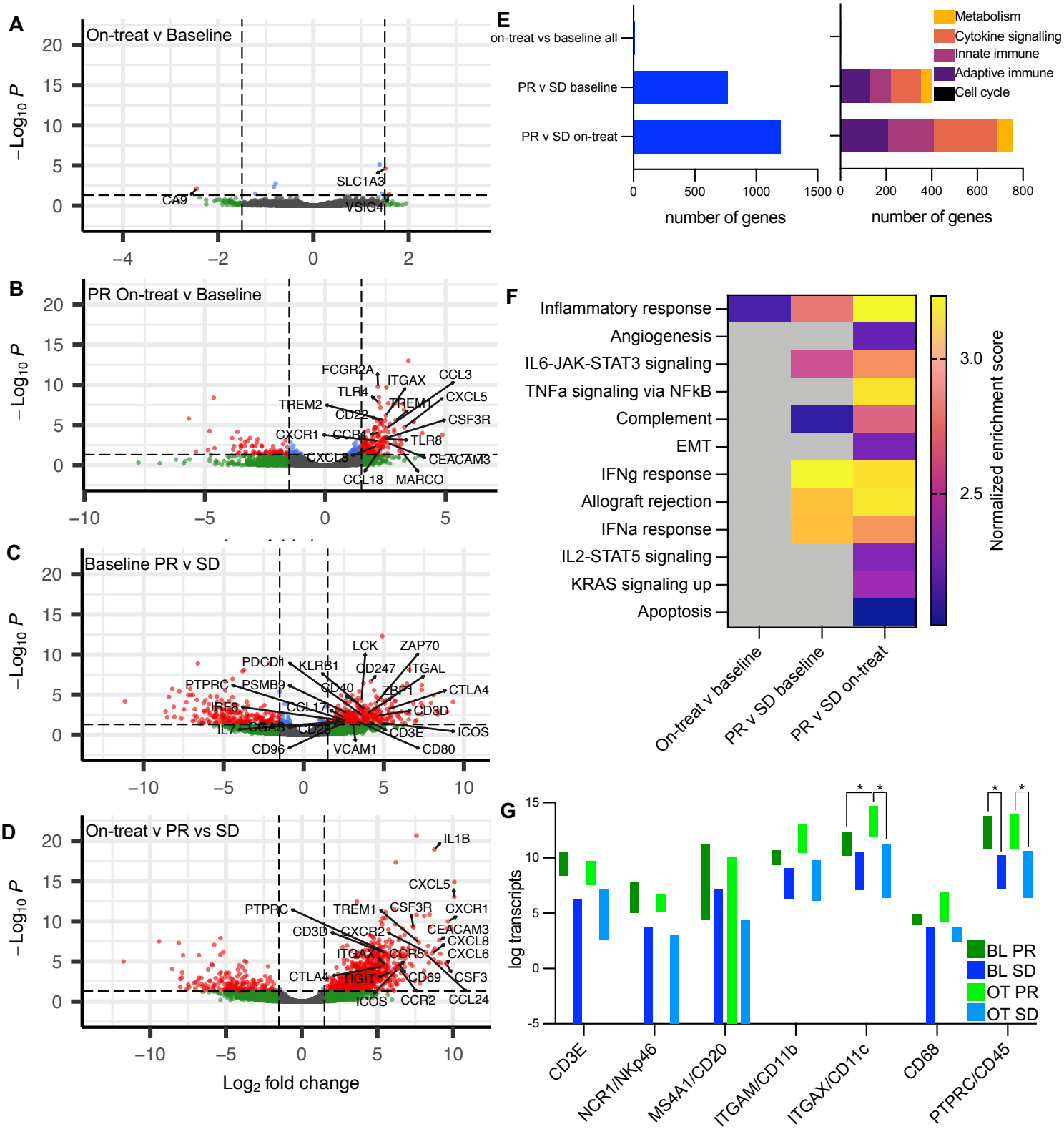
A
On-treat v Baseline
−Log10 P
SLC1A3
CA9
VSIG4
B
PR On-treat v Baseline
FCGR2A
ITGAX
CCL3
TLR4
CXCL5
TREM2
TREM1
CD22
CSF3R
CXCR1
CCR1
TLR8
CXCL8
CEACAM3
CCL18
MARCO
C
Baseline PR v SD
LCK
ZAP70
PDCD1
KLRB1
CD247
ITGAL
PTPRC
PSMB9
CD40
ZBP1
CTLA4
IRF8
CCL17
CD3D
IL7
CGAS
CD28
CD3E
ICOS
CD96
VCAM1
CD80
D
On-treat v PR vs SD
IL1B
CXCL5
PTPRC
TREM1
CSF3R
CXCR1
CD3D
CXCR2
CEACAM3
CXCL8
ITGAX
CCR5
CXCL6
CTLA4
TIGIT
CD69
CSF3
ICOS
CCR2
CCL24
Log2 fold change
E
on-treat vs baseline all
PR v SD baseline
PR v SD on-treat
number of genes
number of genes
Metabolism
Cytokine signalling
Innate immune
Adaptive immune
Cell cycle
F
Inflammatory response
Angiogenesis
IL6-JAK-STAT3 signaling
TNFa signaling via NFkB
Complement
EMT
IFNg response
Allograft rejection
IFNa response
IL2-STAT5 signaling
KRAS signaling up
Apoptosis
On-treat v baseline
PR v SD baseline
PR v SD on-treat
Normalized enrichment score
G
log transcripts
BL PR
BL SD
OT PR
OT SD
CD3E
NCR1/NKp46
MS4A1/CD20
ITGAM/CD11b
ITGAX/CD11c
CD68
PTPRC/CD45

Fig 5

Figure 5: Tumor analysis

A-D: Volcano plots of differential gene expression for the indicated conditions. Log2 fold-change cut-off was set at 2 (1.5 for (A)) and p-value at 0.05. Labelled genes are the most differentially expressed genes which are also present in the REACTOME innate immune, adaptive immune, or immune system gene sets.

A: All samples, on-treatment vs baseline;

B: on-treatment vs baseline in responders;

C: responders vs non-responders, baseline biopsies;

D: responders vs non-responders, on-treatment biopsies.

E: Left: number of significantly differentially expressed genes from paired tumor RNAseq, for the indicated conditions. Right: Number of genes in the indicated REACTOME pathways represented amongst differentially expressed genes for the indicated conditions (not all pathways are shown).

F: GSEA analysis of tumor RNAseq data, using the 'hallmarks' gene set. For the indicated conditions, those pathways with normalized enrichment score >2 are shown. All have nominal p value and FDR q value of 0.000. 'OT': on-treatment; 'BL': baseline; 'PR' partial response; 'SD': stable disease. Heatmap indicates normalized enrichment score for the indicated gene sets.

G: Gene expression (min to max) for the indicated genes, in tumor biopsies at baseline and after 2 weeks' ceralasertib. * $p<0.05$ by 2-way ANOVA.

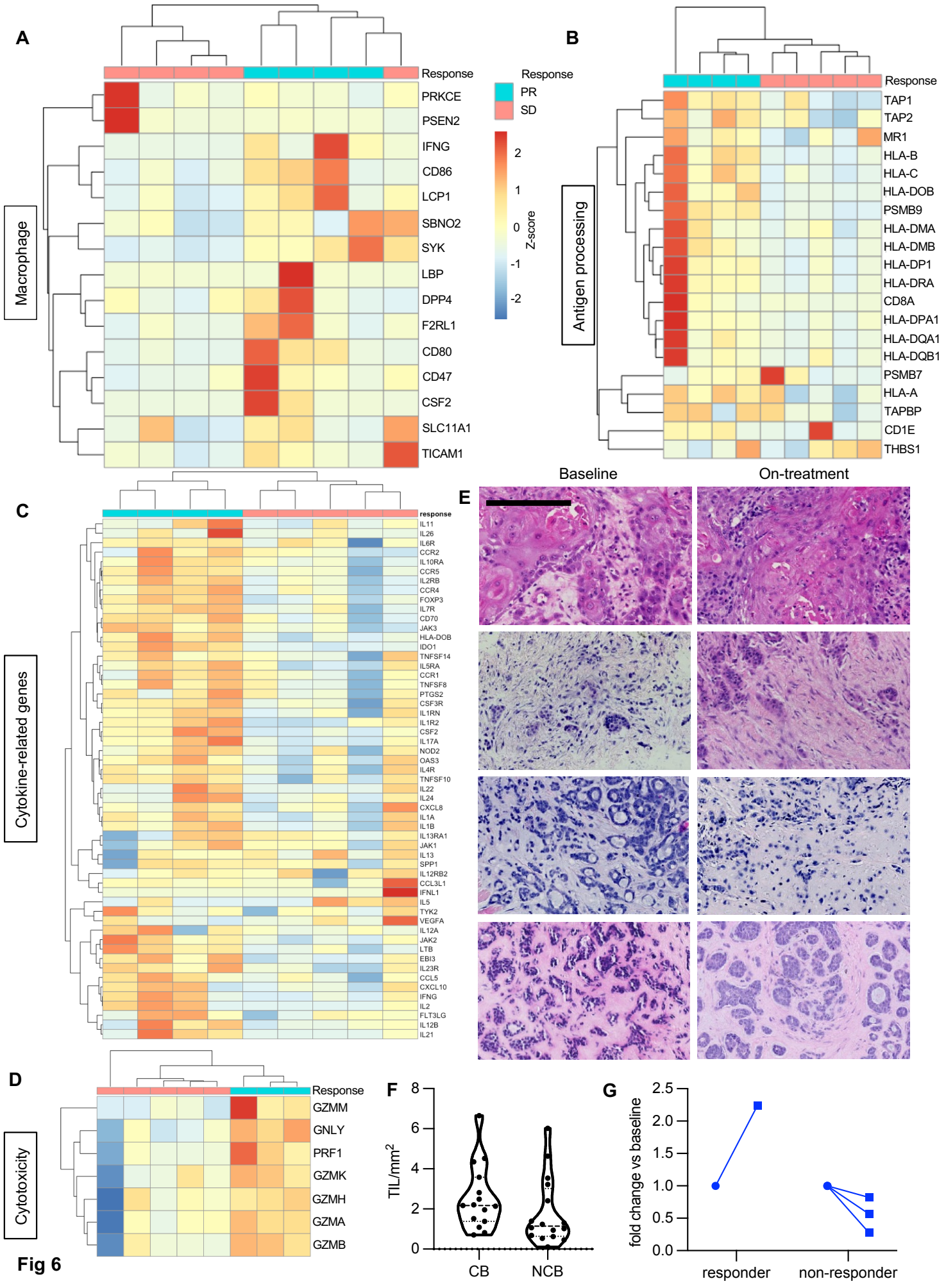
A
Macrophage
Response
PRKCE
PSEN2
IFNG
CD86
LCP1
SBNO2
SYK
LBP
DPP4
F2RL1
CD80
CD47
CSF2
SLC11A1
TICAM1
Response
PR
SD
2
1
0
-1
-2
Z-score
B
Antigen processing
Response
TAP1
TAP2
MR1
HLA-B
HLA-C
HLA-DOB
PSMB9
HLA-DMA
HLA-DMB
HLA-DP1
HLA-DRA
CD8A
HLA-DPA1
HLA-DQA1
HLA-DQB1
PSMB7
HLA-A
TAPBP
CD1E
THBS1
C
Cytokine-related genes
response
IL11
IL26
IL6R
CCR2
IL10RA
CCR5
IL2RB
CCR4
FOXP3
IL7R
CD70
JAK3
HLA-DOB
IDO1
TNFSF14
IL5RA
CCR1
TNFSF8
PTGS2
CSF3R
IL1RN
IL1R2
CSF2
IL17A
NOD2
OAS3
IL4R
TNFSF10
IL22
IL24
CXCL8
IL1A
IL1B
IL13RA1
JAK1
IL13
SPP1
IL12RB2
CCL3L1
IFNL1
IL5
TYK2
VEGFA
IL12A
JAK2
LTB
EBI3
IL23R
CCL5
CXCL10
IFNG
IL2
FLT3LG
IL12B
IL21
Baseline
On-treatment
E
D
Cytotoxicity
Response
GZMM
GNLY
PRF1
GZMK
GZMH
GZMA
GZMB
F
TIL/mm2
8
6
4
2
0
CB
NCB
G
fold change vs baseline
2.5
2.0
1.5
1.0
0.5
0.0
responder
non-responder

Fig 6

Figure 6: Tumor analysis

A: Heatmap of macrophage-related gene expression in baseline tumor biopsies.

B: Heatmap of antigen processing-related transcripts in baseline biopsies. The first column represents the participant shown in fig. 2D, with high mutational burden.

C: Heatmap of cytokine-related gene expression in baseline tumor biopsies. Scale = z-score, scaled by row.

D: Heatmap of cytotoxicity signature in on-treatment biopsies.

E: Representative images of tumor micrographs quantified in (K). Top three rows: participants with stable disease. Lower row: participant with partial response. Scale bar: 200 μm.

F: Stromal tumor-infiltrating lymphocyte count in H&E sections of patients who experienced clinical benefit (CB, defined as partial response or >16 weeks on-study), compared with those who did not.

G: Fold change in stromal tumor-infiltrating lymphocytes in a responding patient and 2 non-responding patients.

Table 1: Baseline characteristics

	Part A (n=26) Number (%)	**Part B (**n=43) Number (%)
Median age (range)	59 (41-80)	57 (36-84)
Female Male	8 (31) 18 (69)	19 (44) 24 (56)
Race White Asian Black Unknown	 24 (92) 1 (4) 1 (4) 0	 37 (86) 4 (9) 1 (2) 1 (2)
Tumor Histology Colorectal SCCHN Other [A] H&N – non-SCC [B] Gynecological – non OCCC [C] Upper gastrointestinal OCCC Lung (non-small cell) Melanoma Prostate Sarcoma	 6 (23) 6 (23) 5 (19) 5 (19) 2 (8) 2 (8) 0 0 0 0 0	 7 (16) 6 (14) 2 (5) 9 (21) 4 (9) 5 (12) 3 (7) 2 (5) 2 (5) 2 (5) 1 (2)
Median prior lines of SACT (range)	4 (1-6)	4 (1-7)

[A] Other histologies: small bowel adenocarcinoma (1), mesothelioma (1), adrenocortical carcinoma (2), eccrine adenocarcinoma (1), digital papillary adenocarcinoma (1), lobular breast carcinoma (1)

[B] Other H&N histologies: acinic cell salivary carcinoma (3), nasopharyngeal carcinoma (2), adenocarcinoma (2), sinonasal carcinoma (1), adenoid ameloblastoma (1), salivary gland carcinoma (1), adenoid cystic carcinoma (2), mucoepidermoid carcinoma (1), nasolacrimal squamous carcinoma (1)

[C] Other gynecological histologies: peritoneal carcinoma (1), serous endometrial carcinoma (2), cervix SCC (1), cervix adenocarcinoma (1), serous ovarian carcinoma (1)

Table 2: TRAEs, judged related to ceralasertib by investigator definitely, probably, or possibly related, by dose level and grade, for all cycles. G1-2 AEs occurring less than 3 times and G3 AEs occurring once are not included. DLTs are described in the text.

	240 mg BD (total n=7)				160 mg BD continuous (total n=12)			160 mg BD intermittent (total n = 35)				80 mg BD (total n = 7)			40 mg BD (total n = 3)		
CTCAE Term	***G1-2***	***G3***	***G4***	***Total***	***G1-2***	***G 3***	***Total***	***G1-2***	***G 3***	***G 4***	*Total*	***G1-2***	***G 3***	*Total*	*G1-2*	*G3*	*Total*
Overall Events: n (%)	26	8	7	34	44	5	49	100	11	1	112	18	5	23	7	0	7
Fatigue	4	1		5	10		10	11	5		16	4		4	2		2
Anemia	3	1	1	5	4	4	8	16	3		19	1	1	2			
Nausea	2	2		0	5		5	15			15	2		2	1		1
Platelet count decreased	1		3	4	3		3	10	1	1	12	1	1	2	1		1
Anorexia	2			2	6		6	6			6	1		1			
Vomiting	1	1		0	1		1	6			6	2		2			
Lymphocyte count decreased	1	1	1	3				3	1		4		2	2			
Neutrophil count decreased	1	1	1	3	1		1	4			4						
White blood cell decreased	1	1		2	1	1	2	3			3						
Constipation					2		2	1			1	1		1	1		1
Diarrhea					1		1	3			3				1		1
Dysgeusia	1			1	1		1	2			2	1		1			
Dizziness								5			5						
Headache	1			1	1		1	3			3						
Dyspnoea					2		2	2			2	1		1			
Rash maculo-papular	1			1				1			1	1		1	1		1
Lethargy	1			1	2		2	1			1						
Epistaxis	2			2				1			1	1		1			
Weight loss	1				2		2					1		1			
Dry mouth								2			2	1		1			
Alkaline phosphatase increased	1			1				1	1		2						
Aspartate aminotransferase increased	1			1				2			2						
Cough	1			1	2		2										
Serum amylase increased			1	1				1			1						
Syncope								1			1		1	1			

Supplementary materials and methods

Key inclusion and exclusion criteria

1. Part B only: documented disease progression prior to study entry and measurable disease by RECIST 1.1 within 4 weeks of study entry
2. Presence of putative markers of sensitivity to AZD6738 defined on analysis of tumor material (for part B only).
3. Evidence of measurable or evaluable disease by RECIST 1.1
4. Patients must have normal organ and bone marrow function measured within 7 days prior to administration of study treatment as defined below:
    - Hemoglobin ≥9.0 g/dL
    - Absolute neutrophil count (ANC) ≥ 1.5 x 10^9/L
    - White blood cells (WBC) > 3x10^9/L
    - Platelet count ≥ 100 x 10^9/L
    - Albumin >30g/L
    - AST and ALT <3 times ULN
    - Total bilirubin <1.5 times ULN
    - PT/APTT (<1.5 x upper limit of normal)
    - INR < 1.5 and no other evidence of impaired hepatic synthetic function
    - Glomerular filtration rate (GFR) >50mL/min, as assessed using the standard methodology at the investigating center (i.e., Cockcroft-Gault, MDRD or CKD-EPI formulae, EDTA clearance or 24-hour urine collection)
    - Serum creatinine <1.5 times ULN
    - Negative serum pregnancy test for females of childbearing potential
5. Part B only: tumor site amenable to fresh biopsy (clinical or radiologically- guided)
6. Not Receiving, or having received, concomitant medications, herbal supplements and/or foods that significantly modulate CYP3A4 or P-gp activity (wash out periods of two weeks, but three weeks for St. John's Wort).

7. Not pregnant or breast-feeding, not of childbearing potential unless adequate contraception is used.
8. No clinically significant cardiac disease including:
    - pre-existing arrhythmia,
    - Any factor increasing the risk of QTc prolongation or arrhythmia,
    - uncontrolled angina pectoris,
    - Myocardial infarction 1 year prior to study entry,
    - Cardiac failure
9. No symptomatic and progressive or steroid-requiring brain metastases or leptomeningeal disease
10. Not hypertensive (clinically uncontrolled, or requiring 2 or more antihypertensive agents)
11. No hypotension or orthostatic hypotension
12. No hematuria (+++ on microscopy or dipstick)

Pharmacokinetics

Plasma samples (50 μL) were analyzed using validated bioanalytical methods for ceralasertib and its metabolite AZ13368982, after the addition of deuterated internal standards, by protein precipitation followed by reversed-phase high-performance liquid chromatography with tandem mass spectrometric detection (HPLC-MS/MS)._Concentrations of each analyte were calculated with reference to a calibration series covering the concentration ranges 41.3 to 41,300 ng/mL and 3.98 to 3,980 ng/mL for ceralasertib and AZ13368982, respectively, constructed by adding known amounts of each to control human plasma and processing these standards in parallel with the trial samples. Both pre- and in-study validation was successfully conducted according to the FDA's Guidance for Industry Bioanalytical Method Validation (47). Evaluated PK parameters for ceralasertib included area under the plasma concentration–time curve (AUC), maximum observed plasma concentration (C_{max}), time to C_{max} (t_{max}), and apparent terminal half-life ($t_{1/2}$) calculated as ln/lambda-z where lambda-z (λz) is the apparent terminal phase rate-

constant estimated by linear regression of logarithmically-transformed concentration-versus-time data. A minimum of three data points were used in calculating λz as per AstraZeneca standard operating procedures. Data from multiple dosing were used to derive accumulation ratios based on C_{max} (R_{ace} C_{max}) and AUC(0-8) (R_{ac} AUC_{0-8}) defined as the ratio between C_{max} or AUC(0-8) after multiple dose and C_{max} and AUC(0-8) at day 1. All PK parameters for ceralasertib were derived using non-compartmental analysis (NCA) method in Phoenix WinNonLin v8.3 software or higher where the 'linear up/log down trapezoidal rule' for AUC was applied. All PK concentrations and parameters were listed and summarized as per AstraZeneca standard operating procedures by dose level and by treatment (single or multiple dose).

Sequencing

Formalin-fixed samples were assessed by a pathologist for tumor-rich areas, which were marked for microdissection at extraction, and tumor content estimated. Tumor and normal tissue (DNA extracted from buffy coats) were analyzed where possible (and for all non-archival biopsies) to remove germline variants.

Formalin-fixed paraffin embedded (FFPE) tissue slides, fresh frozen material, and frozen buffy coat samples were extracted for this study.

FFPE slides were reviewed for tumor content by a pathologist and tumor rich areas were marked for macrodissection at extraction. DNA was extracted using from five 10-micron sections of FFPE tumor samples using QIAamp DNA FFPE tissue kit (56404 QIAGEN).

FF samples were extracted using QIAamp DNA Mini kit (51304 QIAGEN).

Frozen buffy coat samples were extracted on Qiagen QIAsymphony SP instrument, using QIAsymphony DNA_Blood_400_V6_DSP protocol, and QIAsymphony DNA Midi Kit (931255, QIAGEN).

DNA was quantified using the Qubit dsDNA High Sensitivity Assay Kit with the Qubit 3.0 Fluorometer (Invitrogen, Carlsbad, CA).

NGS libraries were prepared from 25-400ng DNA using the KAPA HyperPlus Kit (Kapa Biosystems, Wilmington, MA, USA) and IDT UDI 8bp adapters (Integrated DNA Technologies, Coralville, USA), following the manufacturer's protocol, including dual-SPRI size selection of the libraries (250-450 bp). To optimize enrichment and reduce off-target capture, pooled, multiplexed, amplified pre-capture libraries (up to 20 samples per hybridization) were hybridized overnight using 1 µg of total DNA to a custom design of DNA baits complementary to the genomic regions of interest (NimbleGen SeqCap EZ library, Roche, Madison, WI, USA). Hybridized DNA was PCR amplified and products purified using AMPure XP beads (Beckman Coulter, Danvers, MA, USA) and quantified using Qubit dsDNA High Sensitivity Assay Kit with the Qubit 3.0 Fluorometer (Invitrogen, Carlsbad, CA), and High Sensitivity D1000 TapeStation (Agilent, Santa Clara, USA).

Samples were captured using a targeted capture panel (DDR panel) consisting of 173 genes, including multiple potential sensitizers to ATRi, such as DDR genes, and oncogenes (*Supplementary Table 3)*.

Sequencing was performed on a NextSeq (Illumina, San Diego, CA, USA) with 75 bp paired-end reads and v2 chemistry, or NovaSeq6000 with 100 or 150bp paired-end reads and v1 chemistry, according to the manufacturer's instructions.

Sequencing runs were analyzed using an in-house pipeline. For the demultiplexing, Illumina bcl2fastq was used to assign reads for each sample based on the sequencing of 8-bp unique dual indexes. The reads were aligned to the reference genome build GRCh37/Hg19 using Burrows-Wheeler Aligner (BWA-MEM), followed by the marking of PCR duplicates and calculation of various quality control (QC) metrics using Picard. Genome Analysis ToolKit (GATK) was used for realigning around known indels to improve indel calling and base quality

score recalibration for adjusting systematic errors made by the sequencer when estimating quality scores of each base call. HaplotypeCaller is used for variant calling in germline sample (limit of detection ~10%) and Mutect2 is used for tumor-normal paired somatic analysis (limit of detection ~5%). Mutect2 tumor only mode is used for tumor only somatic analysis (limit of detection ~5%). VCF files were then annotated using oncotator (for samples pre-2019) and Personal Cancer Genome Reporter (for post 2019 samples). The potential mutations identified by in-house pipeline were further checked manually on IGV. Copy number variant was estimated by generalizing the coverage expected for a copy of any given targeted region (i.e.an exon), taking the average coverage across all captured regions to estimate the average coverage of one targeted region. Any ratio below 0.5-fold was defined as a potential deletion, whereas a ratio above 2.4 was flagged as a potential amplification if 80% of the target regions had exceeded the thresholds. Manta and Pindel was used for the detection of structural variants including large indels, potential fusions and ITDs.

For whole exome sequencing, genomic DNA was extracted from Buffy Coat using the Qiagen DNeasy Blood & Tissue Kit, from Frozen Solid Tumors using the Qiagen All Prep DNA/RNA Micro Kit, and from FFPE samples using the Covaris truXTRAC FFPE DNA Kit.
All genomic DNA (200-1000ng) was fragmented to 200bp using a Covaris E Series and the resultant libraries were subjected to DNA Capture using SureSelect XT Human All Exon v5 or v6 kit (Agilent) following the manufacturer's instructions.
Final libraries were quantified using qPCR and clustered at a molarity of 14.5 pM; sequencing was performed on an Illumina HiSeq 2500 using 2x101 cycles of version 2 RAPID SBS chemistry. Tumor samples were sequenced at 100-150x depth and germline samples at 40-60x. Tumor mutational burden was defined as total number of somatic mutations, including

synonymous mutations, divided by the library panel size. Tumor mutational burden was defined as high (≥20 mutations/Mb), intermediate (10-20) or low (<10).

In part B, sequencing of archival tumor material, or external sequencing reports were used to select some patients for the study. Out of 21 archival/external sequencing, confirmatory sequencing using fresh biopsies was performed in 20 tumors, and was concordant in 10 (in 2, the gene of interest was not included on the sequencing panel; in 3, confirmatory sequencing found other mutations of interest, in 5, confirmatory sequencing found no mutations of interest).

Tumor RNAseq

RNA samples were quality-controlled and sequenced by the ICR Genomics Facility. RNA polyA method was used for mRNA selection. Strand-specific libraries were generated using the NEB ultra II directional kit. Illumina paired-end libraries were sequenced on a NovaSeq (Illumina) using Novaseq chemistry acquiring 100bp paired-end (PE) reads. Bcl2fastq software (v2.2.20, Illumina) was used for converting the raw base calls to fastqs and to de-multiplex further the sequencing data. The PE fastq files were used for further analysis. The STAR alignment software (v.2.7.6a) was used to align reads to the reference genome (GRCh38). Once the reads were aligned, HTSeq-count (HTSeq v0.12.4) was used to count the number of reads mapping unambiguously to genomic features in each sample.

Differential expression analysis of the count data was performed in R using the Bioconductor package DESeq2 (v1.34.0). Dispersion estimations were corrected using the fdrtool (v1.2.17). Gene Set Enrichment and Pathway Analysis was carried out in R using DOSE (v3.20.1), pathview (v1.34.0) and clusterProfiler (v4.2.2) packages, and using GSEA (v4.3.2) (48). Volcano plots were generated using EnhancedVolcano v1.16.0. Heatmaps were constructed using the pheatmap package (v1.0.12) using euclidean clustering and scaling by row; gene

signatures for heatmap construction were used from MSigDB (49) and cell-type-related transcripts from NanoString annotations and Bindea et al (50). Cell-type deconvolution was performed using CIBERSORTx (51).

Supplementary Pharmacodynamic methods

IHC

Formalin fixed paraffin-embedded tumor samples were used. Nuclear phospho-$^{(S635)}$Rad50 (Cell Signaling 14223), using a previously published method (52). H-score was calculated using HALO image analysis (Indica Labs). Tumor samples were also stained for γH2AX (S139, Cell Signaling 9718) positivity by IHC. A positive nucleus was defined as one with at least 5 nuclear foci or pan-nuclear staining, resulting in a total percent positive score. Nuclear ATM (Abcam 32420) IHC staining was carried out on the Ventana autostainer, using DAB detection and assessed by H-score, but samples were only deemed acceptable if lymphocyte staining (internal control) was at least 2+ (moderate) intensity. Cyclin E1 (Invitrogen HE12) staining was carried out on the Ventana autostainer, using DAB detection and the H-score was quantified using HALO image analysis (Indica Labs). Ki67 (Mib-1, Dako M7240) was scored by percent nuclear positivity using a global unweighted method, scoring 4 areas of 100 cells. ARID1A IHC was performed as previously published (36), using EPR13501 antibody (Abcam) and scored using H-score for nuclear positivity. Quantification of tumor-infiltrating lymphocytes was done using a semi-automated method in QuPath (53). Scanned H&E sections were first segmented into tumor and stroma, using a random trees machine-learning classifier, for each tumor section. Nuclei were segmented using Stardist (54), then stromal nuclei were sorted by size (area <20 μm^2) and circularity (>0.85), using small circular nuclei to approximate lymphocyte count.

Immunofluorescence

PBMCs were isolated from blood using BD Vacutainer® CPT™ Cell preparation tubes with sodium citrate (BD Biosciences, Wokingham, UK) and fixed with 4% formalin containing 1% Triton™ X-100 (Sigma-Aldrich, St. Louis, MO). PBMC cells were cytospun onto microscope slides and stained with anti-phospho-$^{(S345)}$Chk1 [133D3] (Cell Signaling Technology 2348), or anti-γH2A.X$^{(S139)}$ (Abcam ab11174) antibodies and AlexaFluor 488 goat anti-rabbit IgG antibody (Invitrogen, Carlsbad, CA). Nuclei of PBMCs were counterstained with TOPRO-3 (Invitrogen). A Carl Zeiss LSM 700 confocal laser scanning fluorescence microscope (Zeiss, Jena, Germany) was used to visualize and capture images of the PBMCs. Fluorescent nuclear intensity for phospho-$^{(S345)}$ and total Chk1 in individual PBMC cells were quantified using the IN Cell Investigator Developer Toolbox v1.9 software (GE Healthcare Biosciences, Piscataway, NJ). For the phospho$^{(S345)}$- and total Chk1 assays: the raw data values (fluorescent nuclear intensity for PBMCs), the percentage change for phospho$^{(S345)}$ biomarker was calculated for each subject by comparing the levels measured at each post-dose time point to pre-dose levels measured at baseline. The number of fluorescent γH2AX foci within individual PBMC cells were quantified using the IN Cell Investigator Developer Toolbox v1.9 software and the percentage of cells at each time point with greater than 5 foci calculated. The assays were GCP compliant and utilized healthy volunteer PBMCs as quality controls in every analytical run.

Flow cytometry

Peripheral blood was drawn into 8 mL EDTA tubes (Vacutainer, BD) and analyzed within 24 hours. ACK-lysed whole blood (for myeloid panel) or PBMC from density gradient centrifugation (for lymphocyte panel) were used. Samples were surface-stained with antibodies for 30 mins at

4 ^{o}C. Samples were analyzed on a LSR Fortessa (BD Biosciences). FACS analyses were performed in FlowJo v10.

Antibodies used

Mix 1

NKG2D	BV421	Biolegend
CD4	BV510	Biolegend
CD45	BV650	Biolegend
TCRγδ	FITC	Biolegend
CD25	PE	Biolegend
CD56	PE-Dazzle 594	Biolegend
CD73	APC	Biolegend
CD62L	PerCp Cy5.5	Biolegend
CD3	AF700	Biolegend
CD8	Pe-Cy7	Biolegend
CD127	APC-Cy7	Biolegend

Mix 2:

NKp46	BV421	Biolegend
CD4	BV510	Biolegend
CD45	BV650	Biolegend
TCRγδ	FITC	Biolegend
OX-40	PE	Biolegend
CD56	PE-Dazzle 594	Biolegend
4-1BB	APC	Biolegend
NKp30	PerCp Cy5.5	Biolegend
CD3	AF700	Biolegend
CD8	Pe-Cy7	Biolegend
CD69	APC-Cy7	Biolegend

Mix 3:

NKG2A	BV421	BD
CD4	BV510	Biolegend
CD45	BV650	Biolegend
TCRγδ	FITC	Biolegend
PD-1	PE	Biolegend
CD56	PE-Dazzle 594	Biolegend
LAG-3	APC	R&D Systems
TIGIT	PerCp Cy5.5	eBioscience
CD3	AF700	Biolegend
CD8	Pe-Cy7	Biolegend
TIM-3	APC-Cy7	Biolegend

Mix 4:

CD45RO	Pacific Blue	Biolegend
CD4	BV510	Biolegend
CD45	BV650	Biolegend
CD45RA	FITC	Biolegend
CCR7	PE	Biolegend
CD56	PE-Dazzle 594	Biolegend
CD27	APC	Biolegend
CD62L	PerCp Cy5.5	Biolegend
CD3	AF700	Biolegend
CD8	Pe-Cy7	Biolegend
CD16	APC-Cy7	Biolegend

Mix 5:

CD56	BV421	Biolegend
CD4	BV510	Biolegend
CD45	BV650	Biolegend
TCRγδ	FITC	Biolegend
LAP	PE	Biolegend
CTLA-4	PE-Dazzle 594	Biolegend
ICOS	APC	Biolegend
CD57	PerCp Cy5.5	Biolegend
CD3	AF700	Biolegend
CD8	Pe-Cy7	Biolegend
CD95	APC-Cy7	Biolegend

Mix 6:

PVR	BV421	Biolegend
CD19	BV510	Biolegend
CD45	BV650	Biolegend
CD3	FITC	Biolegend
PD-L1	PE	Biolegend
CD38	PE-Dazzle 594	Biolegend
CD27	APC	Biolegend
CD62L	PerCp Cy5.5	Biolegend
CD14	AF700	Biolegend
HLA-E	Pe-Cy7	Biolegend
CD56	APC-Cy7	Biolegend

Mix 7:

NKG2A	BV421	BD
CD8	BV510	Biolegend
CD45	BV650	Biolegend
CD69	FITC	Biolegend
PD-1	PE	Biolegend
CD38	PE-Dazzle 594	Biolegend
CD56	APC	Biolegend
TIGIT	PerCp Cy5.5	eBioscience
CD3	AF700	Biolegend
CD57	Pe-Cy7	Biolegend
CD16	APC-Cy7	Biolegend

MDSC/DC/monocytes

CD33	P67.6	APC		Biolegend
CD11b	ICRF44	PE		Biolegend
CD11c	3.9	BV421		Biolegend
CD15	HI98	FITC		Biolegend
HLA-DR	L243	PerCP Cy5.5		Biolegend
CD14	M5E2	BV510		Biolegend
CCR2	K036C2	Pe-Cy7		Biolegend
CD16	3G8	APC-C7		Biolegend
Lin (CD3, CD19, CD56)				
CD45	HI30	BV650		Biolegend
Isotype	MOPC-173	AF700		

Gating strategy

See supp Fig. 13, 14

Plasma cytokine analysis

Plasma was taken from EDTA tubes (BD vacutainer) used for buffy coat or immune profiling samples. Plasma was removed, re-spun and aliquoted into 1.5 mL tubes and stored at -70 ^{O}C until analysis. Samples were run in duplicate using the Bio-Plex Pro Human Cytokine 27-plex panel (Bio-Rad) as per manufacturer's instructions.

Criteria for Dose Limiting Toxicity

1. Hematological toxicity
    1. Grade 3 thrombocytopenia with bleeding
    2. Grade 4 thrombocytopenia
    3. Grade 4 neutropenia lasting >7 days in the absence of growth factor support
    4. Grade 4 neutropenia of any duration accompanied by fever ≥ 38.5°C and/or systemic infection
    5. Any other grade ≥4 hematological toxicity
2. Cardiovascular toxicity
    1. Clinically significant hypotension defined as an asymptomatic fall in systolic blood pressure more than 20mmHg to below 70mmHg persisting for at least 10 minutes
    2. Symptomatic orthostatic fall in systolic blood pressure of more than 20mmHg compared to resting supine blood pressure
    3. Prolongation of QTc >0.5 seconds (using an appropriate correction QTcB (Bazzett) or QTcF (Fridericia))
3. Gastrointestinal/hepatic toxicity
    1. ALT or AST >5 times ULN; ALP >5 times ULN with elevated gamma- GT

2. ALT or AST >3 times ULN (or ALP >3 times ULN with elevated gamma-GT) with the appearance of symptoms associated with a clinical diagnosis of hepatitis including right upper quadrant pain or tenderness, fever, rash, or eosinophilia (>5%)
3. [ALT or AST >3 times ULN] and [total bilirubin >2 times ULN] or INR >1.5x ULN (unless patient receiving warfarin) (or other evidence of impaired liver synthetic function)

4. Any other grade 3-4 non-hematological toxicity occurring during the time period from the first dose to the end of the first cycle
    1. Excluding grade 3 diarrhea which resolves to grade 1 within 24 hours of medical management
    2. Excluding grade 3 nausea or vomiting if ameliorated by medical management
    3. Excluding grade 3 fatigue unless there is an increase by 2 grades from baseline
5. Any dose in cycle 1, or the start of cycle 2, delayed by more than 7 days due to toxicity or patient unable to complete cycle 1 at the planned dose due to toxicity (parts A and B only)
6. Any other toxicity that is greater than baseline, is clinically significant and/or unacceptable, does not respond to supportive care, results in a disruption of dosing schedule of more than 14 days or is considered to be dose-limiting by the investigators.

List of supplementary figures and tables

Supplementary References

47. *Guidance for Industry, Bioanalytical Method Validation, U.S. Department of Health and Human Services, Food and Drug Administration, Center for Drug Evaluation and Research (CDER), Center for Veterinary Medicine (CMV)*. Rockville, MD: Food and Drug Administration; 2018.
48. Subramanian A, Tamayo P, Mootha VK, Mukherjee S, Ebert BL, Gillette MA, et al. Gene set enrichment analysis: a knowledge-based approach for interpreting genome-wide expression profiles. *Proceedings of the National Academy of Sciences of the United States of America.* 2005;102(43):15545-50.
49. Liberzon A, Birger C, Thorvaldsdóttir H, Ghandi M, Mesirov JP, and Tamayo P. The Molecular Signatures Database (MSigDB) hallmark gene set collection. *Cell Syst.* 2015;1(6):417-25.
50. Bindea G, Mlecnik B, Tosolini M, Kirilovsky A, Waldner M, Obenauf AC, et al. Spatiotemporal dynamics of intratumoral immune cells reveal the immune landscape in human cancer. *Immunity.* 2013;39(4):782-95.
51. Newman AM, Steen CB, Liu CL, Gentles AJ, Chaudhuri AA, Scherer F, et al. Determining cell type abundance and expression from bulk tissues with digital cytometry. *Nat Biotechnol.* 2019;37(7):773-82.
52. Jones GN, Rooney C, Griffin N, Roudier M, Young LA, Garcia-Trinidad A, et al. pRAD50: a novel and clinically applicable pharmacodynamic biomarker of both ATM and ATR inhibition identified using mass spectrometry and immunohistochemistry. *British journal of cancer.* 2018.
53. Bankhead P, Loughrey MB, Fernández JA, Dombrowski Y, McArt DG, Dunne PD, et al. QuPath: Open source software for digital pathology image analysis. *Scientific Reports.* 2017;7(1):16878.
54. Schmidt U, Weigert M, Broaddus C, and Myers G. In: Frangi AF, Schnabel JA, Davatzikos C, Alberola-López C, and Fichtinger G eds. *Medical Image Computing and Computer Assisted Intervention – MICCAI 2018*. Cham: Springer International Publishing; 2018:265-73.

List of supplementary figures and tables

Supp Fig1: Bone marrow toxicity, by dose and schedule

Supp Fig 2: Accumulation ratios

Supp Fig 3: Change in PBMC phospho-(S345)Chk1 fluorescence intensity after 2-week treatment

Supp Fig 4: Tumor kinetics for participants at 1 site (Royal Marsden).

Supp Fig 5: Duration on study by mutational status.

Supp Fig 6: Oncoprint of more detailed mutational information, sorted by duration on study.

Supp Fig 7: Tumour mutational burden, by clinical benefit

Supp Fig 8A, B: Heatmap of top 100 differentially expressed genes, in baseline biopsies

Supp Fig 9: Geneset enrichment analysis using the 'Hallmarks' gene set.

Supp Fig 10: CIBERSORTx cell-type deconvolution data, by response

Supp Fig 11: cell-type signatures.

A: T-cell functions signature, baseline biopsies

B: NK cell function signature, baseline biopsies

C: cytokine signature, on-treatment biopsies

D: T-cell functions signature, on-treatment biopsies

Supp Fig 12: Interferon-stimulated gene signature.

Supp Fig 13: Flow cytometry gating strategy for monocytes, MDSC, and DC

Supp Fig 14: Lymphocyte gating strategy

Supp Table 1: SAE related to ceralasertib (judged by investigator as definitely, probably or possibly related).

Supp Table 2: Dose-limiting toxicities

Supp Table 3: Genes of interest in sequencing panel, used for selection.

Supp table 4: SWI/SNF mutations

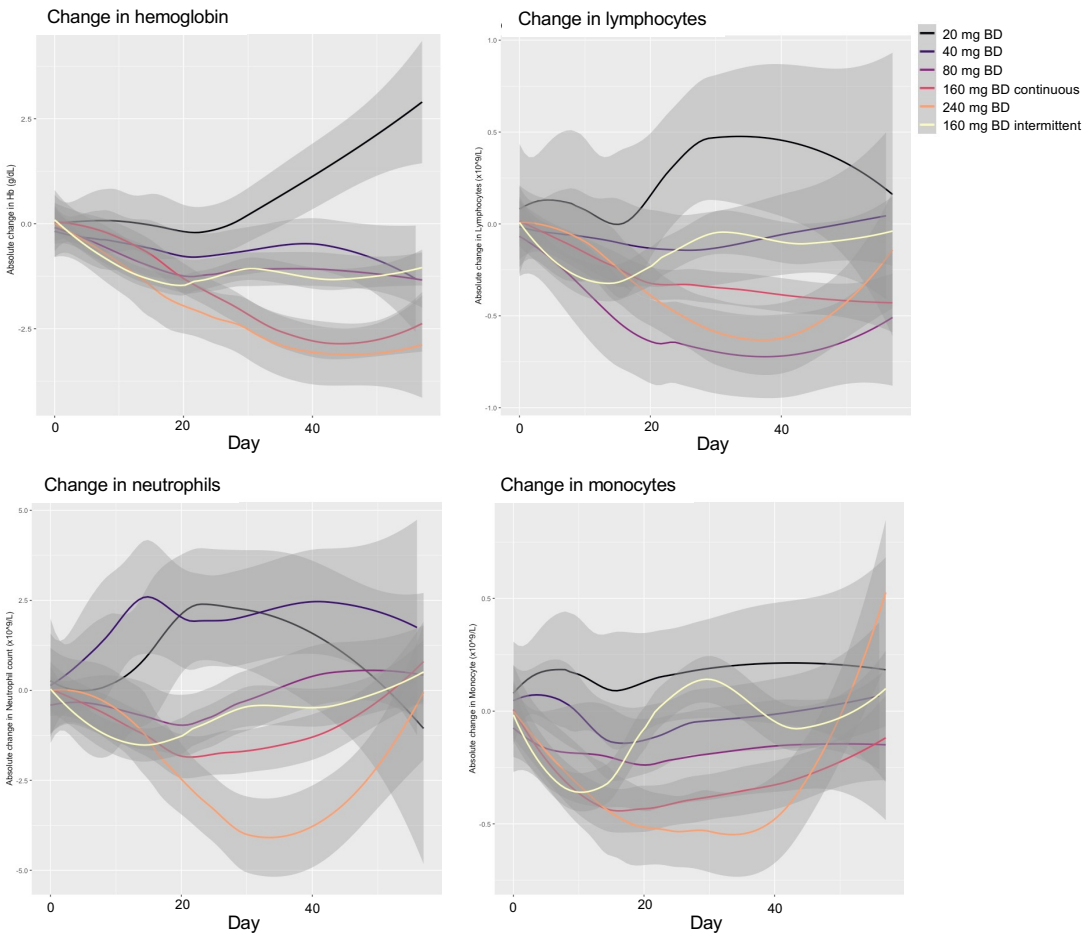

Supp Fig 1
Bone marrow toxicity, by dose and schedule
Change in full blood count parameters with time, by dose cohort. Smoothed conditional mean absolute changes compared with baseline blood count are presented, with 95% CI.

CTCAE term	240 mg BD	160 mg BD continuous	160mg BD Intermittent	80 mg BD
Anemia	1, G4	1, G2	1, G3	1, G3
Platelet count decreased	2, G4			
Blood bilirubin increased			1, G3	
Increased amylase	1, G3			
Non-cardiac chest pain		1, G3		
Urinary tract infection		1, G3		
Electrocardiogram QTc interval prolonged		1, G1		
Syncope			1, G3	1, G3
Left ventricular systolic dysfunction		1, G3		
Pneumonitis	1, G2			
Photosensitivity	1, G3			

Supp Table 1
SAE related to ceralasertib (judged by investigator as definitely, probably or possibly related). No related SAE at 20 and 40 mg dose levels

Dose cohort	Number in cohort evaluable for DLT	DLT	Number of DLT
20 mg BD	3	none	0
40 mg BD	3	none	0
80 mg BD	6	Thrombocytopenia, G3 with epistaxis (n=1)	1
160 mg BD	6	none	0
240 mg BD	6	Increased amylase, G3 (n=1), thrombocytopenia G4 (n=2)	3

Supp Table 2
Dose-limiting toxicities

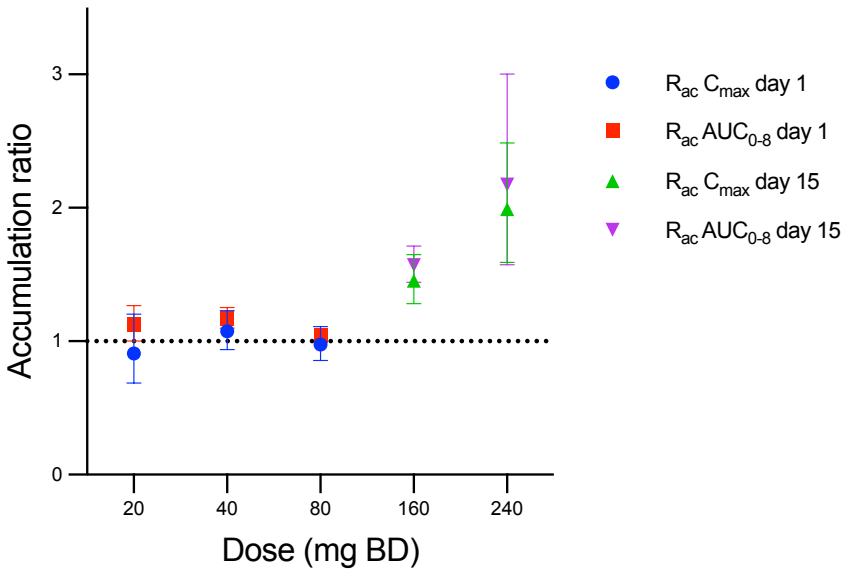

Supp Fig 2
Accumulation ratios
accumulation ratio of ceralasertib, calculated by geometric mean Cmax or AUC0-8 at day 1 vs. day 0, or day 15 vs. day 0 for the indicated dose levels.

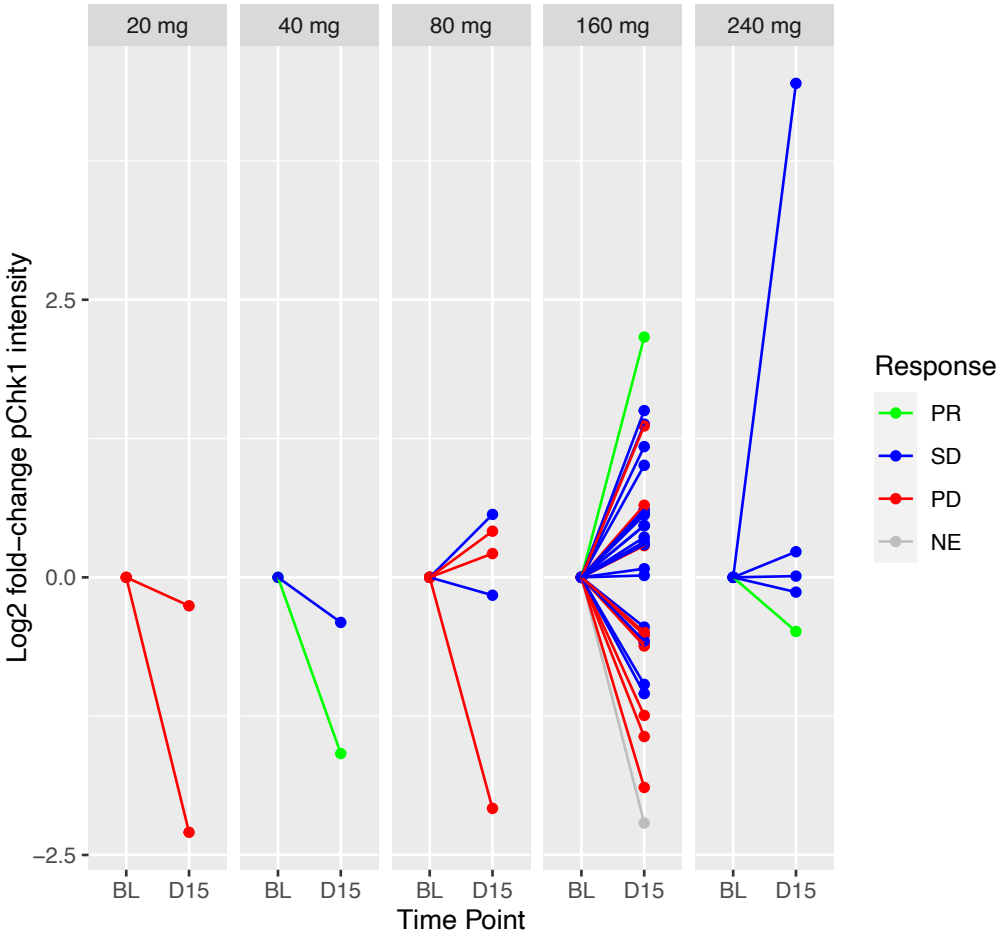

Supp Fig 3
Change in PBMC phospho-(S345)Chk1 fluorescence intensity after 2-week treatment (D15), normalized to baseline (BL) per patient, by dose level. Color of line indicates RECIST response.

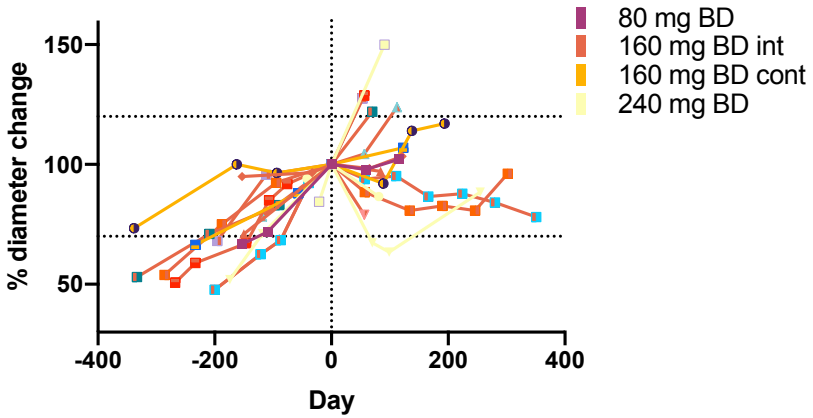

Supp Fig 4: tumor kinetics for participants at 1 site (Royal Marsden). Medical records were reviewed to obtain prior tumor measurements (negative days) for the target lesions. These were taken and normalized to the baseline measurements for this study (day 0 measurement).

ATM-G1	ATR	CIN	DSB	EXCISION	FANC	HR	MMR
ATM*	ATR	AURKA	CDK12	LIG1	C17orf70 / FA	BABAM1	MLH1
CDKN1A (p2	ATRIP	POLD1*	H2AFX	LIG4	DNA2	BARD1	MLH3
CDKN2A (p1	ATRX	POLD2	RNF168		FANCA	BRCA1	MSH2
CDKN2B	CDC25A	POLD3	SLX4*	RECOVERY	FANCB	BRCA2	MSH3
CHEK2	CDC25C	POLD4		BLM	FANCC	BRIP1	MSH6
KAT5	CHEK1	POLE		EME1	FANCD2	DCLRE1C	PMS2
MDC1	CLSPN	PTEN		MUS81	FANCE	EXO1	RECQL
MDM2	HUS1			WRN	FANCF	GEN1	
MDM4	RAD1	NER	NHEJ	SWI/SNF	FANCG	PALB2*	ONCOGENE
MRE11A	RAD17	ERCC1*	SETMAR	ARID1A*	FANCI	PARP1*	BRAF
NBN	RAD9A	ERCC4*	TP53BP1*	ARID1B	FANCL	PARP2	CCND1
PRKDC	RBBP8	XRCC1*	XRCC5	ARID2	FANCM	Rad51	CCNE1*
RAD50	RPA1		XRCC6	SMARCA4	XRCC2	RAD51AP1	HRAS
TP53	TOPBP1			SMARCB1		RAD51B	KRAS
						RAD51C	MYC*
					TLS	RAD51D	MYCL*
					MAD2L2	RAD54B	MYCN*
					REV3L*	RAD54L	NRAS
						XRCC3	
						XRCC4	

Supp Table 3: genes of interest in sequencing panel, used for selection. * Signifies those with published data to support ATRi sensitization

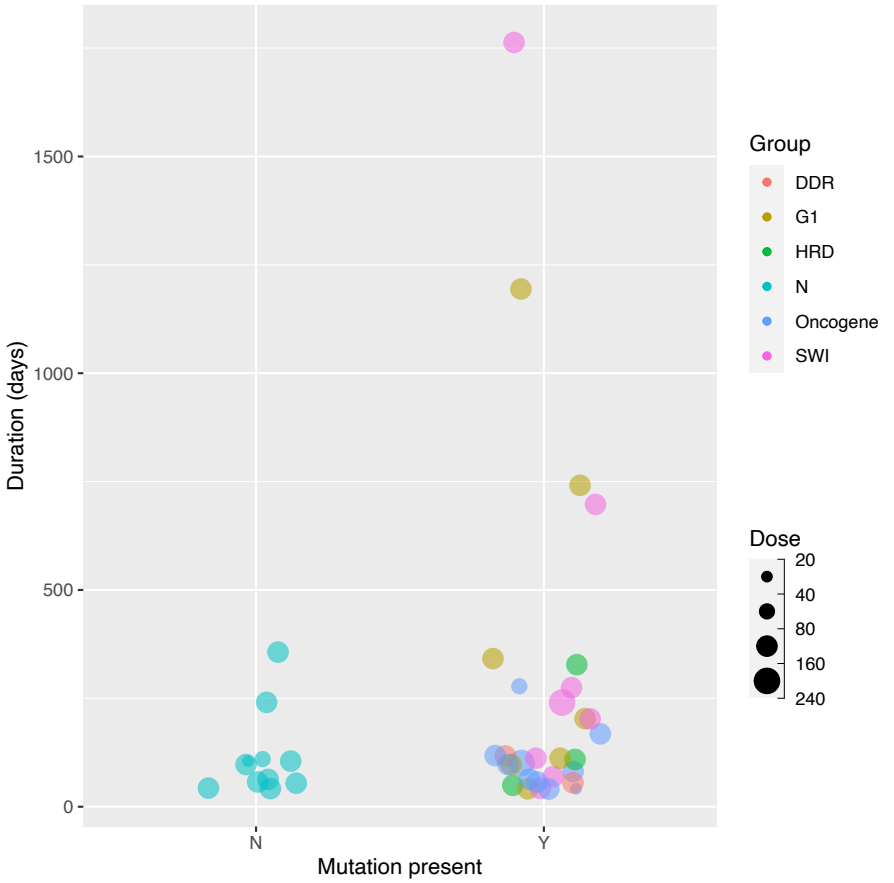

Supp Fig 5
Duration on study by mutational status. DDR: DNA damage response defect (not otherwise mentioned); G1: ATM -G1 pathway; HRD: homologous recombination pathway; Oncogene: driver mutation; SWI: SWI/SNF pathway mutation; N = no mutation. Participants who had available sequencing data for their tumors were included. If sequencing was not done, they were not included. Mutation of interest defined in Supp. Table 3.

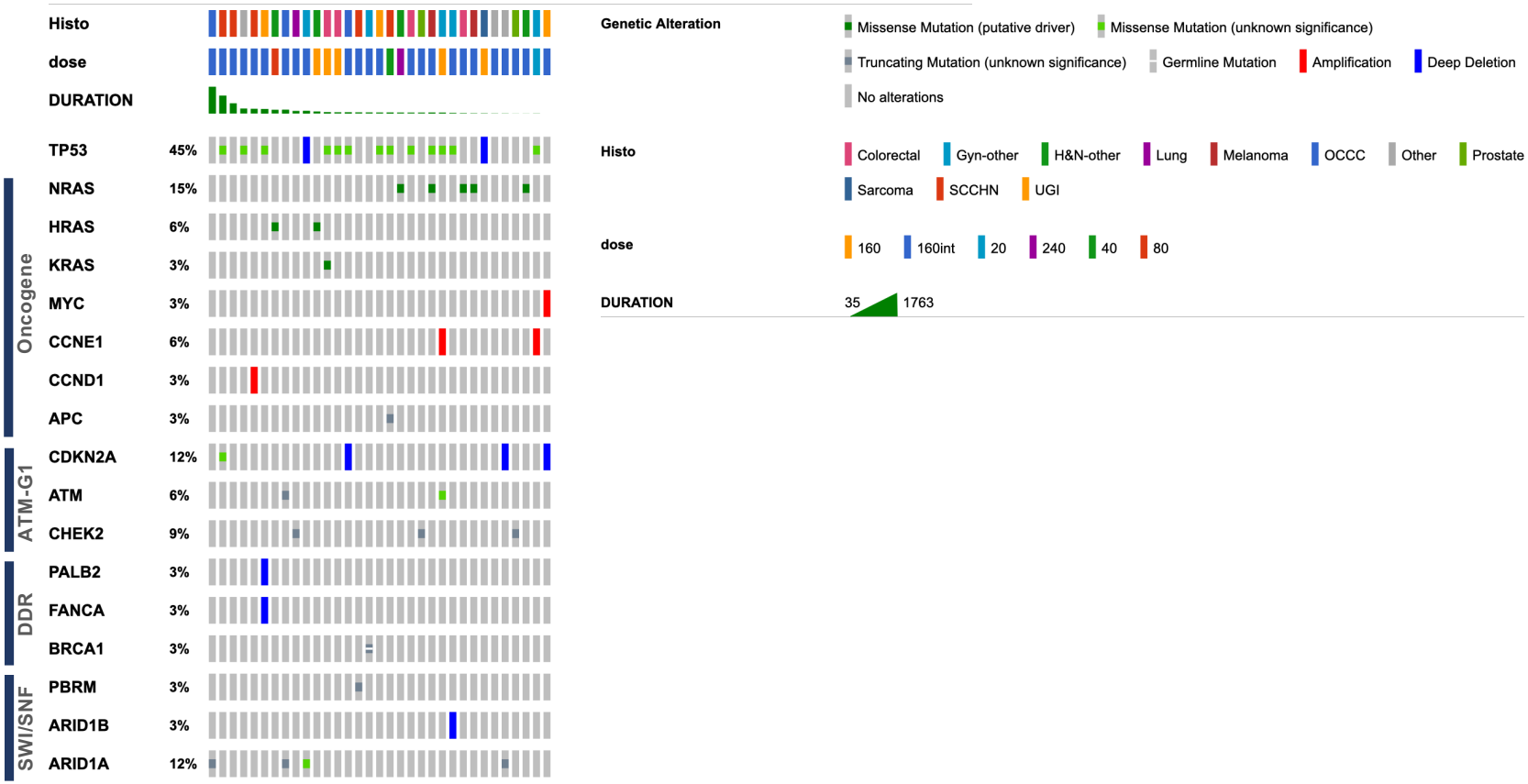

Supp Fig 6
Oncoprint of more detailed mutational information, sorted by duration on study. Oncoprint generated using cBioPortal [44].

Gene	Mutation	Mutation type	Protein loss	Histology	Response	Duration (d)	Coexisting mutation	TMB (mut/Mb)
ARID1A	E1763fs	Frameshift	Yes (H 0)	Ovarian clear cell (Fig. 3J)	PR	1763	PI3KCA missense	70.97
ARID1A	R693*	Truncating	Yes (H 0)	Eccrine adenocarcinoma (Fig. 3K)	SD	240		13.33
ARID1A	S1623L	Missense	No (H 300)	Cervix adenocarcinoma (Fig. 3M)	SD	203	SMARCA4 loss, cyclin E overexpression	9.37
ARID1A	Q1188X	Missense	No (H 235)	Ovarian clear cell (Fig. 3N)	SD	275	ATM frameshift, 50% ATM+ (protein)	12.05
ARID1A	E1387X	Missense	No (H 290)	Lobular breast carcinoma (Fig. 3L)	PD	42	CDKN2A loss	18.75
PBRM	S295*	Truncating	unknown	SCCHN	SD	112		5.36
ARID2	Y854fs	Frameshift	Unknown	SCCHN	SD	697		10.71

Supp table 4
SWI/SNF mutations
TMB: tumor mutational burden.

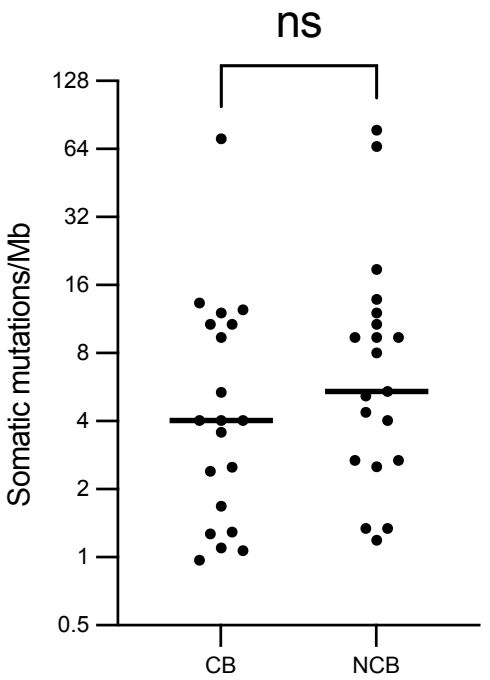

Supp Fig 7
Tumor mutational burden, where available.
CB: clinical benefit, defined as best response of RECIST PR or RECIST SD for 112 days or more
NCB: no clinical benefit, defined as best response of RECIST PD or RECIST SD for less than 112 days.

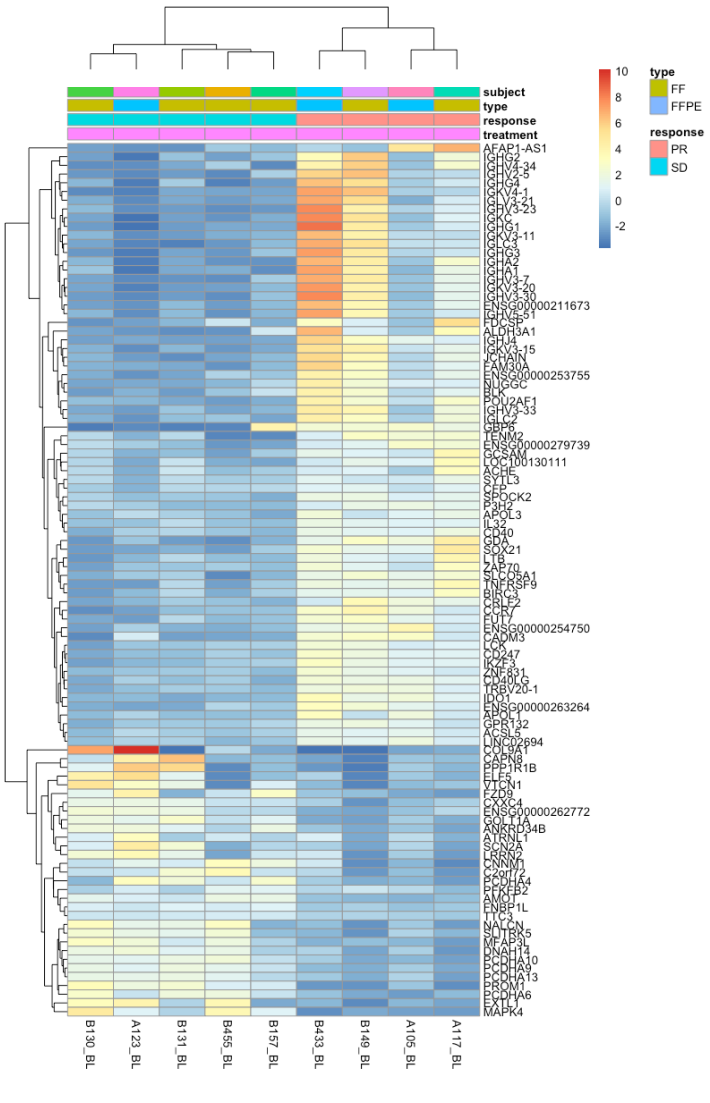

Supp Fig 8A (left) B (right)
Heatmap of top 100 differentially expressed genes, in baseline biopsies
Heatmap of top 100 differentially expressed genes with the lowest adjusted p-value, clustering according to response for (A) baseline and (B) on-treatment tumor biopsies. The data are rlog transformed.

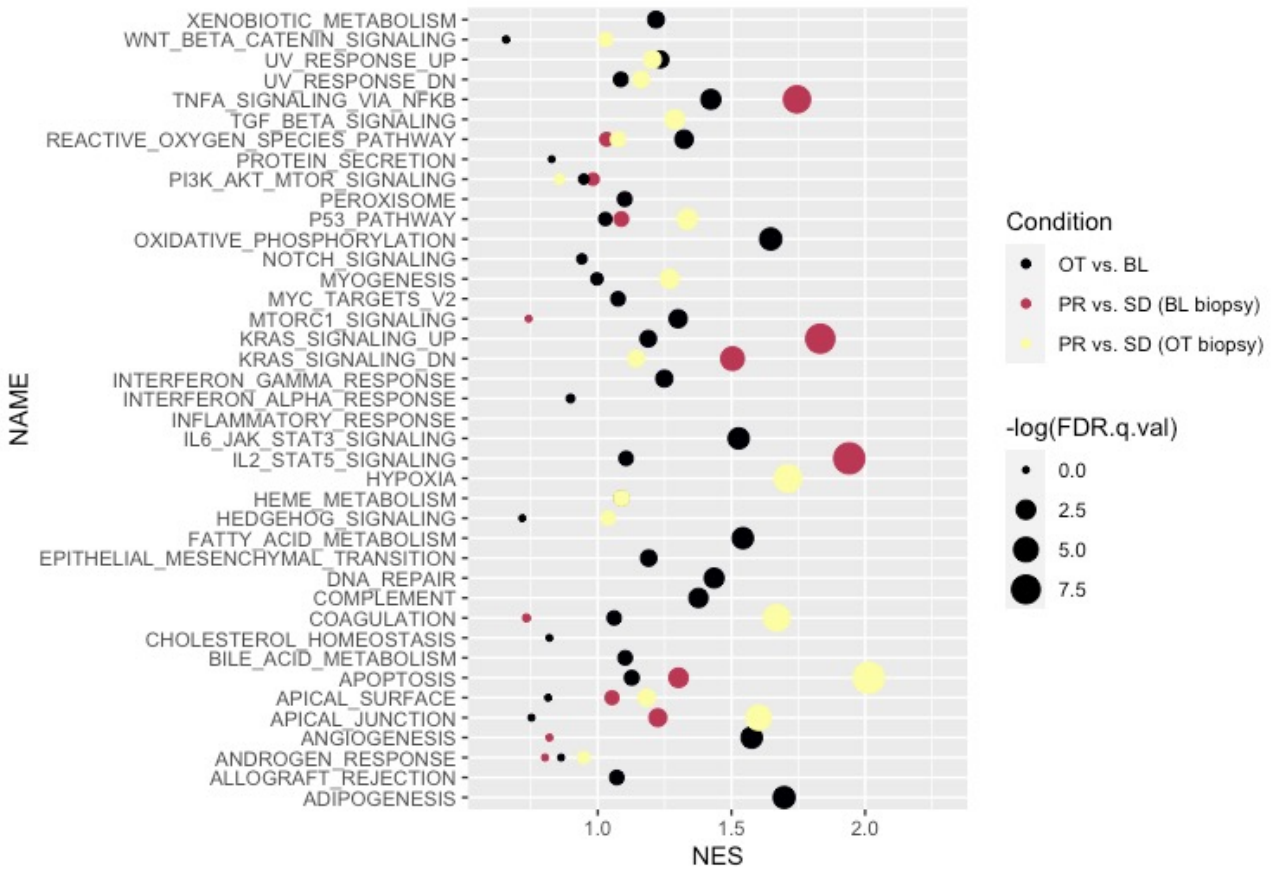

Supp Fig 9

Geneset enrichment analysis using the 'Hallmarks' gene set.

Pathway analysis of differentially expressed genes. Gene set enrichment analysis was carried out using the 'hallmarks' gene set. Normalized expression data for each condition was used from DEseq2. Conditions: OT vs. BL: all samples, on-treatment vs. baseline biopsy; PR vs. SD (BL biopsy): differences between patients having RECIST partial response (PR) or stable disease (SD) i.e., responders vs non-responders, comparing baseline biopsies; PR vs. SD (OT biopsy) difference between responders and non-responders, comparing on-treatment biopsies. Color indicates condition, size indicates false discovery rate q-value, 'NES': normalized enrichment score.

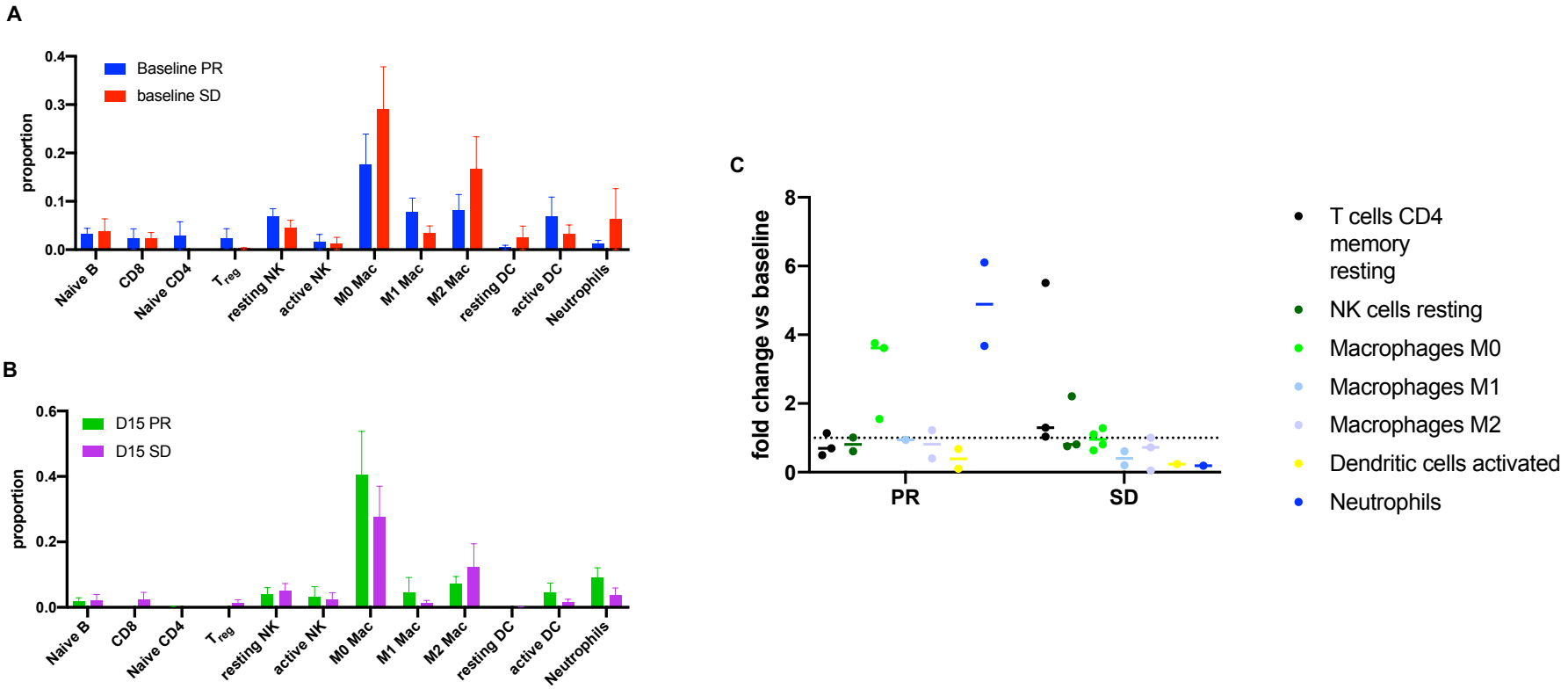

Supp Fig 10
CIBERSORTx cell-type deconvolution data, by response
A: Baseline samples, split by RECIST response
B: On-treatment samples, split by RECIST response
C: Fold-change in cell type proportion (on-treatment divided by baseline) split by RECIST response

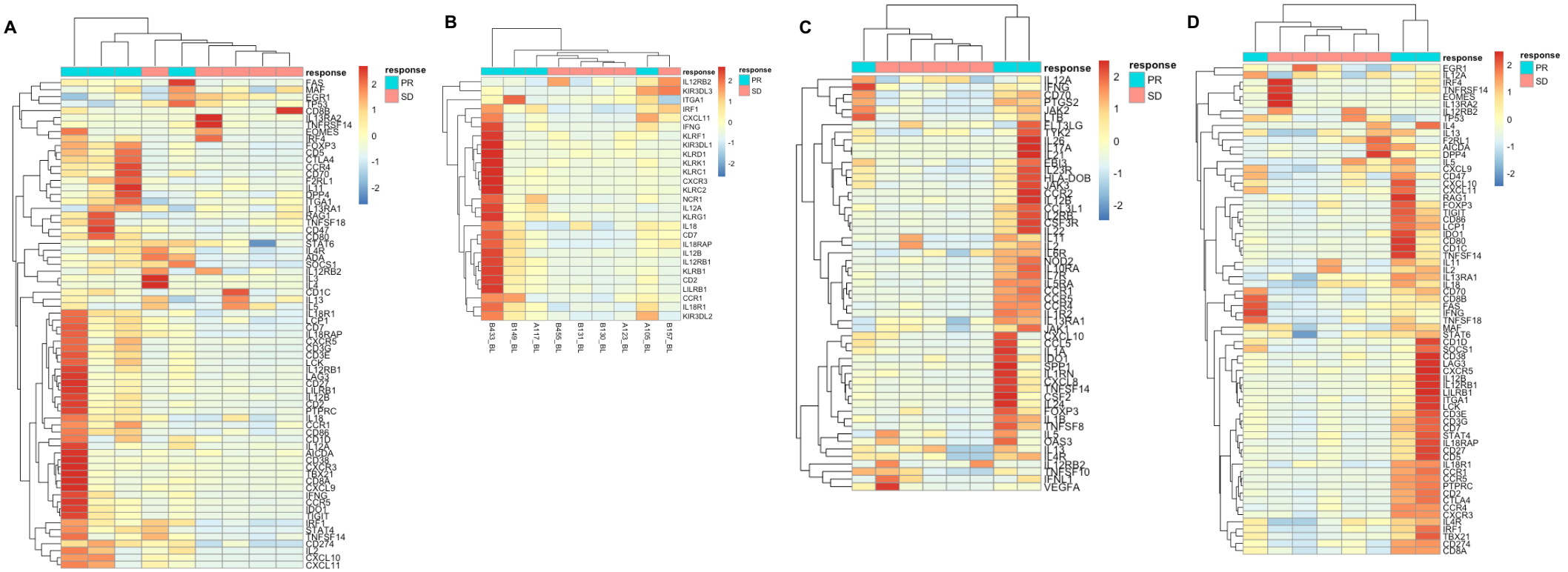

Supp Fig 11: cell-type signatures.

A: T-cell functions signature, baseline biopsies

B: NK cell function signature, baseline biopsies

C: cytokine signature, on-treatment biopsies

D: T-cell functions signature, on-treatment biopsies

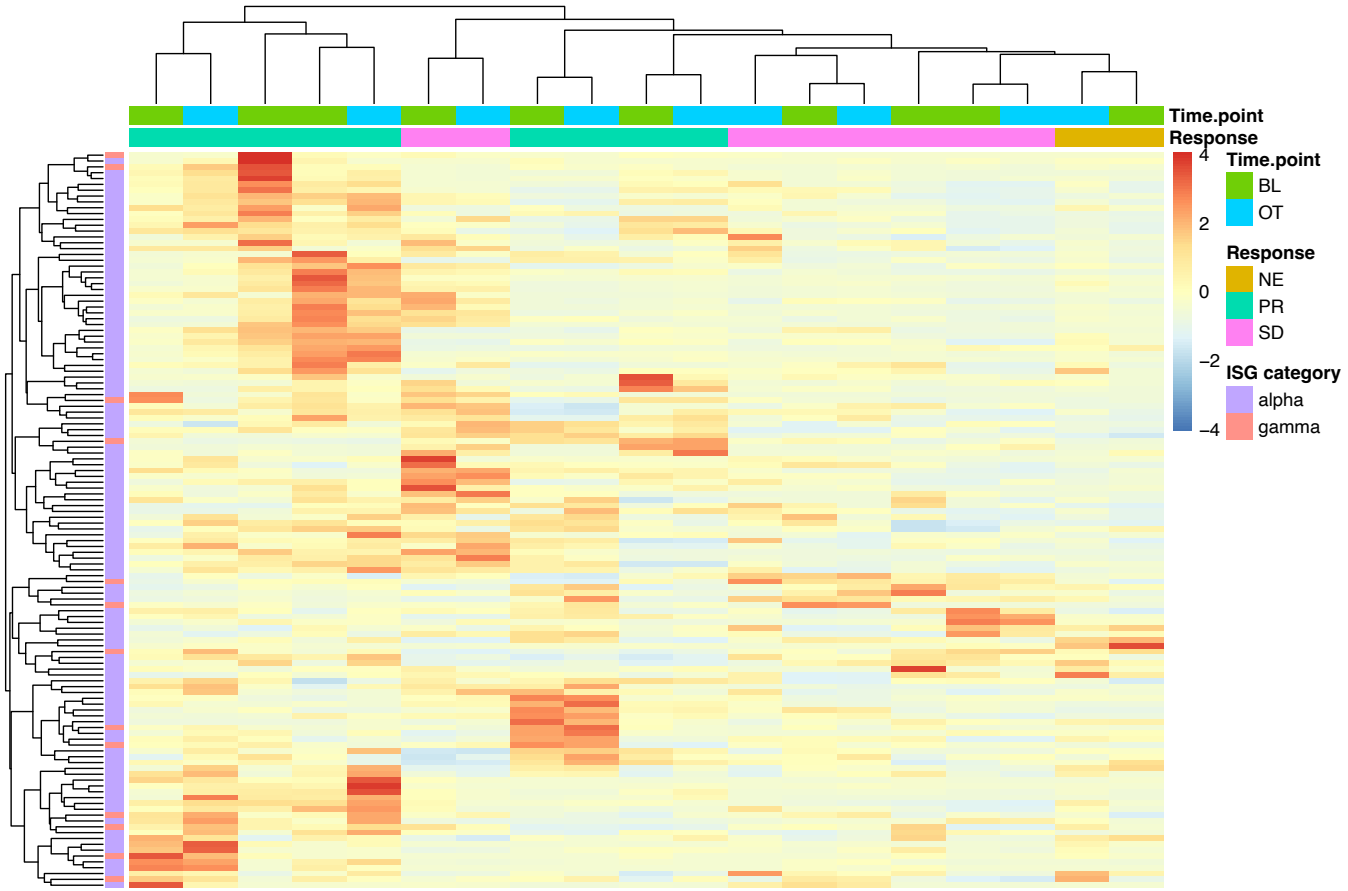

Supp Fig 12: Interferon-stimulated gene signature. Interferon-stimulated genes, and categorisation by alpha or gamma interferon stimulation were obtained from Liu et al., 2011, PNAS 109(11): 4239. “NE” indicates a patient who was not evaluable for response assessment. ”BL” baseline biopsy, “OT” on-treatment biopsy (generally day 15)

Supp Fig 13
flow cytometry gating strategy for monocytes, MDSC, and DC

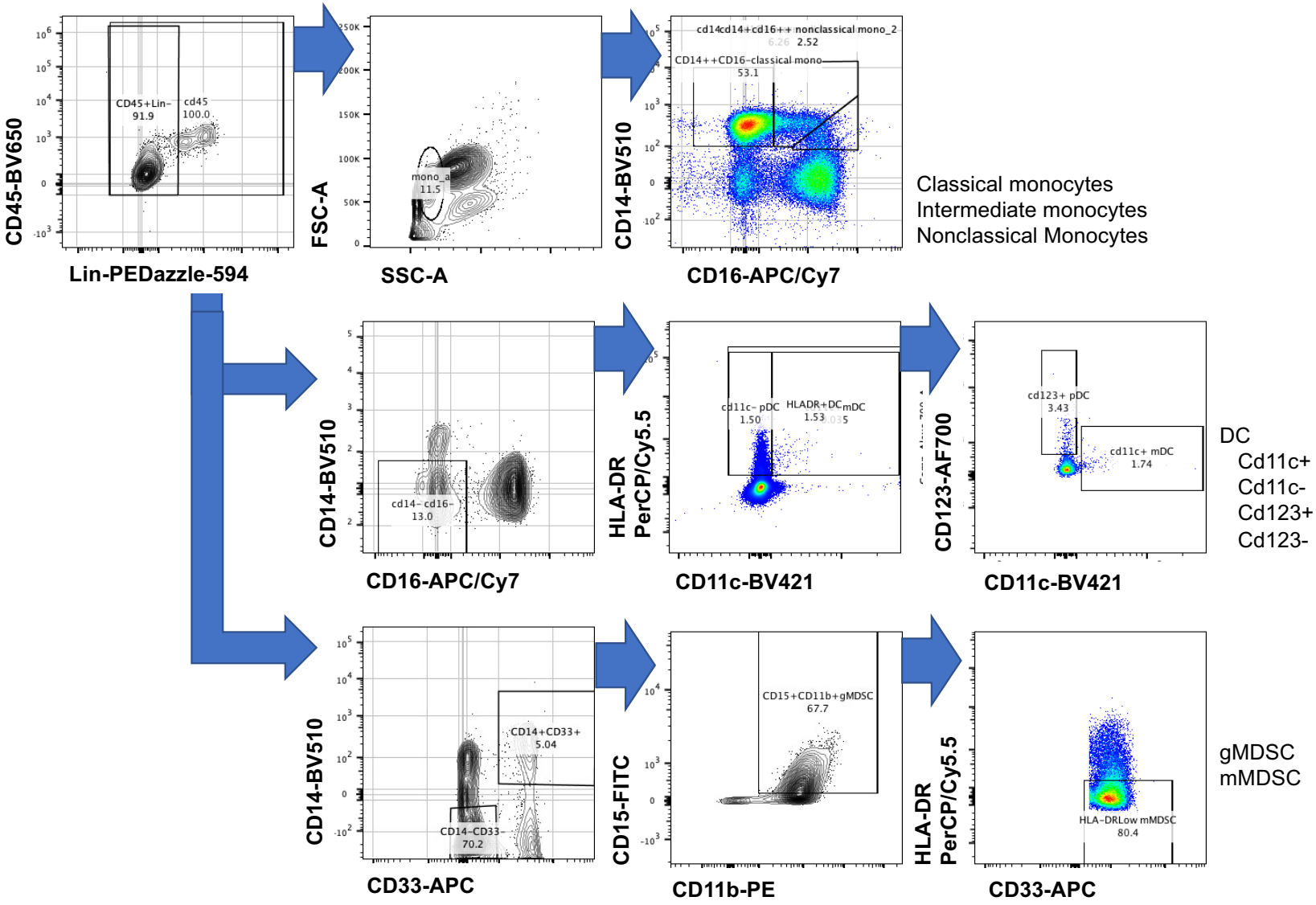

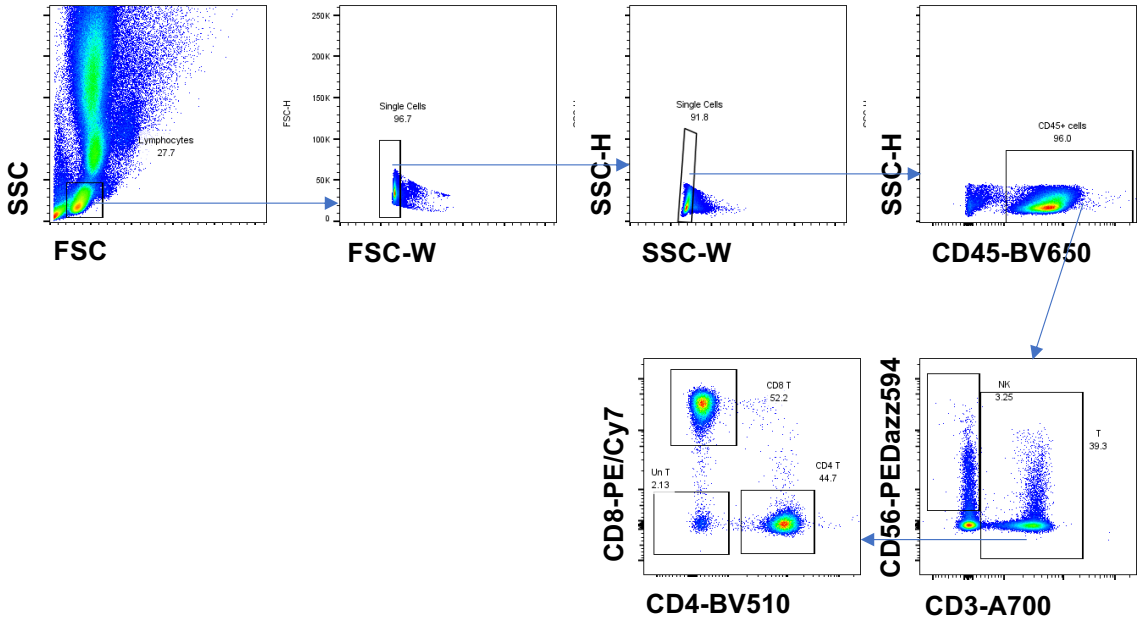

Supp Fig 14
Lymphocyte gating strategy